7 TELESCOPE STRUCTURE

7.1 Introduction

The challenge of designing a stiff telescope structure becomes more difficult as the telescope's size increases. For a reasonable family of design choices, the modal performance and the ability to resist disturbances such as wind shake naturally decrease with increasing structure size. Wind acting on the structure and optics will perturb the alignment of the optics and telescope pointing. These disturbances will be resisted by the telescope structure and drives. Any residual errors require correction by the fast steering and/or adaptive optics systems of the telescope which must be designed with sufficient bandwidth and stroke to handle these errors. The best of the current generation of large telescopes (Magellan, LBT) have lowest vibration modes around 8 Hz. The lowest fundamental modes on 20-30 meter extremely large telescopes (ELTs) will be in the range of 2-5 Hz, with typical control bandwidths of the telescope drives a factor of 2-4 less. This gets down to a range of frequencies where wind disturbance has increasingly significant power and where attenuation and correction of disturbances with the telescope structure and drives becomes less effective. GMT will rely on a combination of structure stiffness and active/adaptive control of the optics to mitigate these effects.

All modern large telescopes use active closed-loop control to achieve optimum alignment of the telescope optics. This task is easier on a stiff structure with low hysteresis where the non-thermal deflections are smaller and the required interval between corrections is correspondingly longer. GMT will have multiple nested control loops for maintaining optical alignment as described in Chapter 8.

Costs for the telescope structure and mechanisms will generally scale with the mass of the telescope. Minimizing these costs is essential for a telescope 2.5-4 times the size of the current generation of large telescopes and requires an exceptionally efficient structure in terms of stiffness to weight. The choice of materials, use of standard and commercially available components, fabrication techniques and the means for transporting the telescope parts to the site are all factors in the cost that have been considered in the conceptual design.

The increased mass of the telescope also creates a problem for thermal conditions in the dome. Heat released as the structure cools during the night will contribute to blurring of the images (dome seeing). The heat will be flushed from the enclosure with wind-driven ventilation through the enclosure doors and vent openings. Minimizing the telescope and enclosure mass will reduce the ventilation requirements and wind loading on the telescope. Reducing the thermal settling time by use of plate steel as thin as practical for the structure and active cooling of the primary mirror assembly will promote rapid equilibration with the outside ambient air temperature.

The GMT goal is to design a telescope structure as compact and stiff as practical within the constraints set by the optical design and size of planned and future instruments. The design

scales up the successful Magellan and LBT concepts that both use welded plate construction and large diameter elevation journals for efficient load transfer to the foundation.

The remainder of this chapter describes the GMT requirements and structure and mechanism designs in greater detail. Results of static, modal and dynamic modeling of the structure are presented.

7.2 **Overview**

GMT uses an altitude over azimuth telescope configuration, Figure 7-1, common to all of the current generation fully steerable large telescopes. The structure is designed to be compact and efficient with high stiffness, minimal top-end cross section to wind disturbance and good thermal performance. The fast f/0.7 focal ratio of the primary mirror reduces the length of the central telescope structure compared to slower optical designs contributing to the overall compactness.

Figure 7-1. Giant Magellan Telescope.

As optical telescopes get larger there is a natural tendency for the primary mirror assembly to constitute an increasing percentage of the mass in the Optical Support Structure (OSS). For the Magellan 6.5 Meter telescopes, the primary mirror and cell, including support and ventilation systems, constitute about 40% of the OSS assembly weight. For GMT that number has increased to nearly 60%. This fact tends to place the center of balance for the structure at the height of the

primary mirror. If the altitude axis is placed forward of the primary mirror (M1) assembly, the OSS is inherently back-end heavy. If it is located behind the M1 assembly (especially far enough behind to exit a usable coaxial Nasmyth beam with instrument clearance) the OSS is inherently front-end heavy. In either case one would have to add weight and dimension to the OSS just to balance it about the altitude axis in addition to the weight and moment loads required for the platforms themselves. If the platforms are placed behind the primary mirror, almost half of the available space is precluded by the motion of the primary mirrors as the OSS rotates in elevation.

For these reasons the GMT Project decided not to implement the Nasmyth foci. We have instead located the altitude axis where it most efficiently balances the OSS. Instruments will be mounted below the center primary mirror segment on the Instrument Platform (IP) (Figure 7-2). The center of the IP consists of an 8.9-meter rotator table and guider assembly. Permanently mounted small- to intermediate-size instruments will be placed on top of the IP and the telescope beam will be directed to them by folding flats. The folded ports will allow rapid instrument changes and a stable platform for precision AO systems. A service lift in the "observing" floor will lift instruments onto the IP from the level of the azimuth turntable.

Larger instruments (e.g. the visible-band multi-object spectrograph) and those that require a minimum number of warm reflections (e.g. the near-IR multi-object spectrograph) will attach to the bottom of the IP at the Gregorian focus. Instruments up to 6.4 m in diameter, 7.6 m tall, and weighing 23 metric tons can be accommodated. They will be exchanged from below using an elevator in the center of the pier.

Relaying the beam with a fold mirror above the primary mirror assembly to an Instrument Platform outside the diameter of the mirrors was considered. This would significantly add to the diameter of the telescope and enclosure with a negative impact on cost and performance. Other complications also argued against this approach for GMT.

The segmented secondary mirror assembly will be supported by a hybrid truss structure that combines high stiffness and a very small thermal footprint, only shadowing 9% of the central segment and none of the outer segments. The secondary mirror assembly will be suspended below the frame at the top of the truss with a hexapod for positioning. The geometry of the truss allows the six off-axis primary mirror assemblies to be lifted out of the telescope using the overhead crane in the enclosure. The center mirror assembly will be removed using the central elevator.

The primary mirror segments will be removed from the telescope in their cells for re-coating the reflective surfaces. An extra 7^{th} off-axis primary mirror assembly will allow swapping of cells to minimize telescope down-time. This requires that the outer cells be rotationally symmetric. No extra central mirror is planned. Procedures for cleaning and washing the mirrors are described in Section 10.11.

Most of the structure of GMT will be fabricated from steel. Steel has the advantages of good stiffness, low cost, and widely available fabricators. A combination of welded plate construction and tubular trusses has been chosen to optimize the stiffness. Plate and structural tube wall

thicknesses are kept to a minimum to allow rapid thermal equilibration with the ambient air. The upper truss members, where high stiffness to weight is critical, are made of carbon fiber.

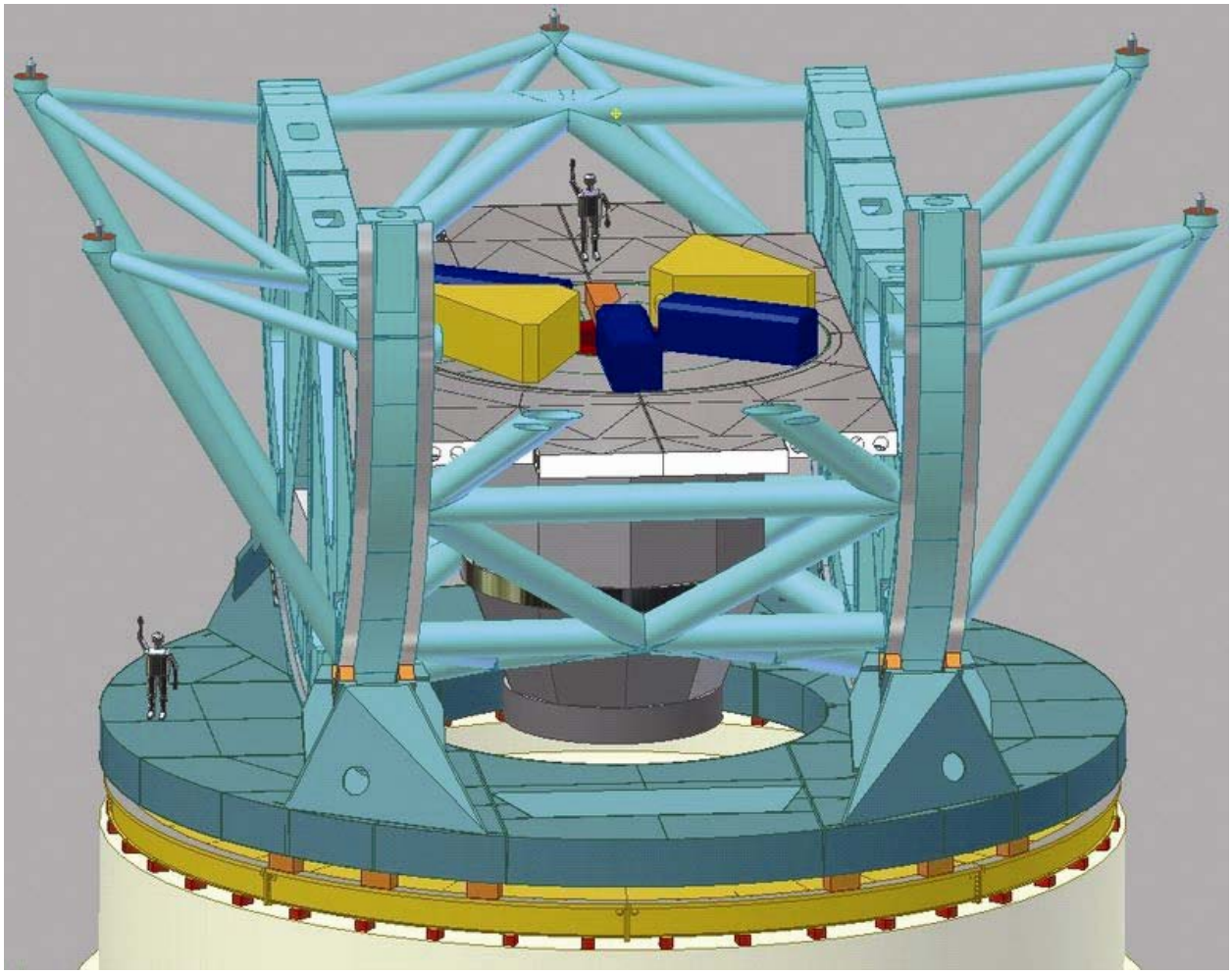

Figure 7-2. Instrument Mounting.

7.3 **Requirements & Specifications**

The GMT mount provides the support for the telescope instruments and optics with the ability to acquire and track astronomical objects over the visible sky above a minimum specified elevation angle. Figure 7-3 gives dimensions for the telescope and pier.

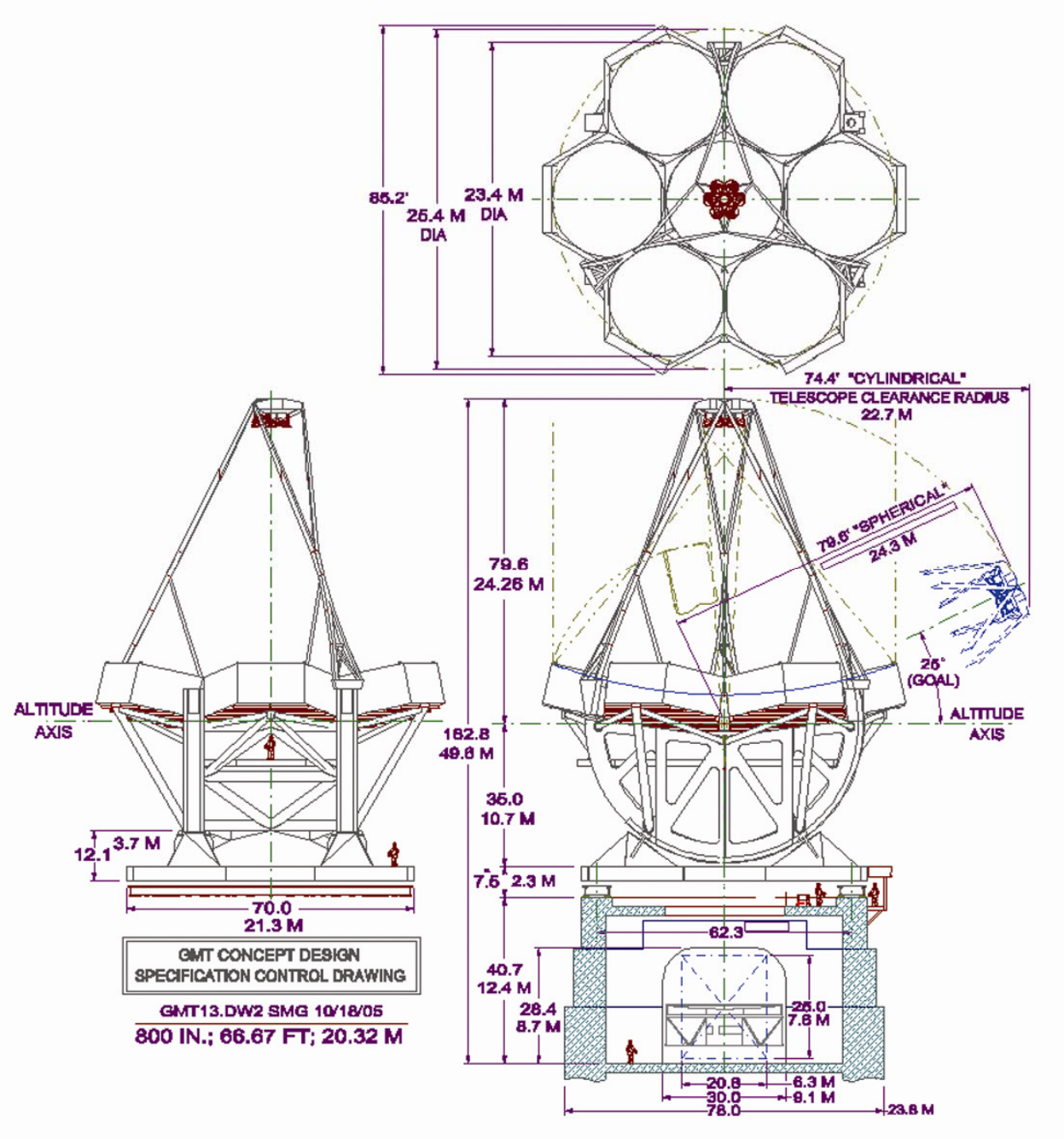

Figure 7-3. GMT dimensions.

The GMT mount is essentially a 2-axis altitude-over-azimuth gimbal. Hydrostatic bearings running on large diameter machined journals define the rotation axes. Instruments are mounted on an Instrument Rotator (IR) that compensates for field rotation in the alt-az design and is part

of the Instrument Platform below the primary mirror. The telescope and rotator motions are specified in Table 7-1.

Table 7-1. GMT axis motion specifications.

Parameters	Specification	Goal
Azimuth Axis:		
Observing range	$\pm$255°	
Rotation rate	-1.2°/sec to +1.2°/sec	-1.7°/sec to +1.7°/sec
Acceleration	-0.1°/sec^2 to +0.1°/sec^2	
Slew time, 180°	190 sec	135 sec
Altitude Axis:		
Observing range, elevation	30.0° to 89.5°	27.0° to 89.5°
Rotation rate	-0.9°/sec to +0.9°/sec	-1.2°/sec to +1.2°/sec
Acceleration	-0.1°/sec^2 to +0.1°/sec^2	
Slew time, 60°	88 sec	70 sec
Instrument Rotator:		
Observing range	$\pm$180°	
Rotation rate	-1.2°/sec to +1.2°/sec	-2.2°/sec to +2.2°/sec
Acceleration	-0.2°/sec^2 to +0.2°/sec^2	-0.4°/sec^2 to +0.4°/sec^2
Slew time, 180°	185 sec	100 sec
Blind pointing accuracy		
Offsets $\leq$ 1°	$\leq$ 0.3 arc-sec rms	$\leq$ 0.2 arc-sec rms
1° < Offset $\leq$ 10°	$\leq$ 2.0 arc-sec rms	$\leq$ 1.0 arc-sec rms
Offsets > 10°	$\leq$ 3.0 arc-sec rms	$\leq$ 2.0 arc-sec rms
Tracking accuracy, 60s unguided		
RMS	$\leq$ 0.03 arc-sec	
Peak-to-valley	$\leq$ 0.15 arc-sec	

The complete set of top level functional and performance specifications for the GMT mechanical structure including thermal and service requirements is given in Section 3 of the "Giant Magellan Telescope Design Requirements Document," GMT Document 292 provided as Appendix 7-1 to this document.

7.4 **Main Structure**

Typical of altitude-over-azimuth mounts, the GMT structure consists of two rotating structural assemblies, the optics support structure (OSS) and the azimuth structure. Each assembly is made up of component structures which are described below. The one non-rotating part of the telescope is the azimuth track, described in section 7.4.7. The pier which provides the connection between the telescope and the ground is not formally part of the telescope structure but is critical for the overall stiffness and modal performance of GMT. It is discussed in section 7.5.

7.4.1 OSS structures

As shown in Figure 7-4 and Figure 7-5, the OSS consists of three distinct structures: the c-ring assembly, the primary mirror structure assembly, and the secondary truss.

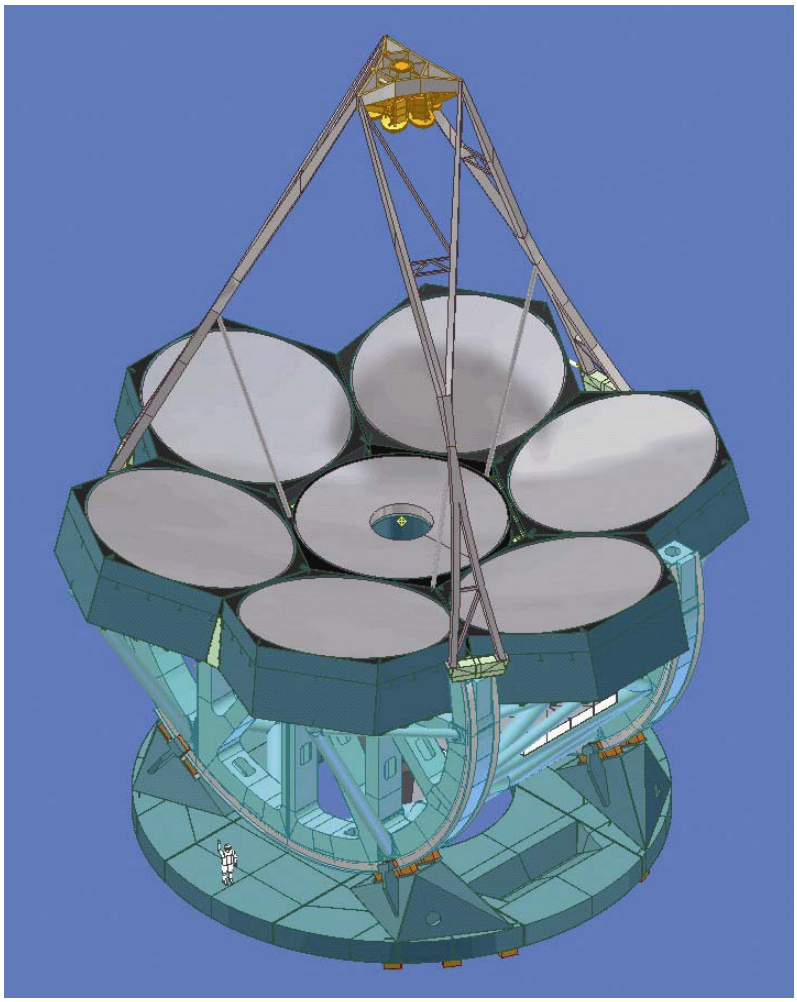

Figure 7-4. Upper view of rotating telescope structure.

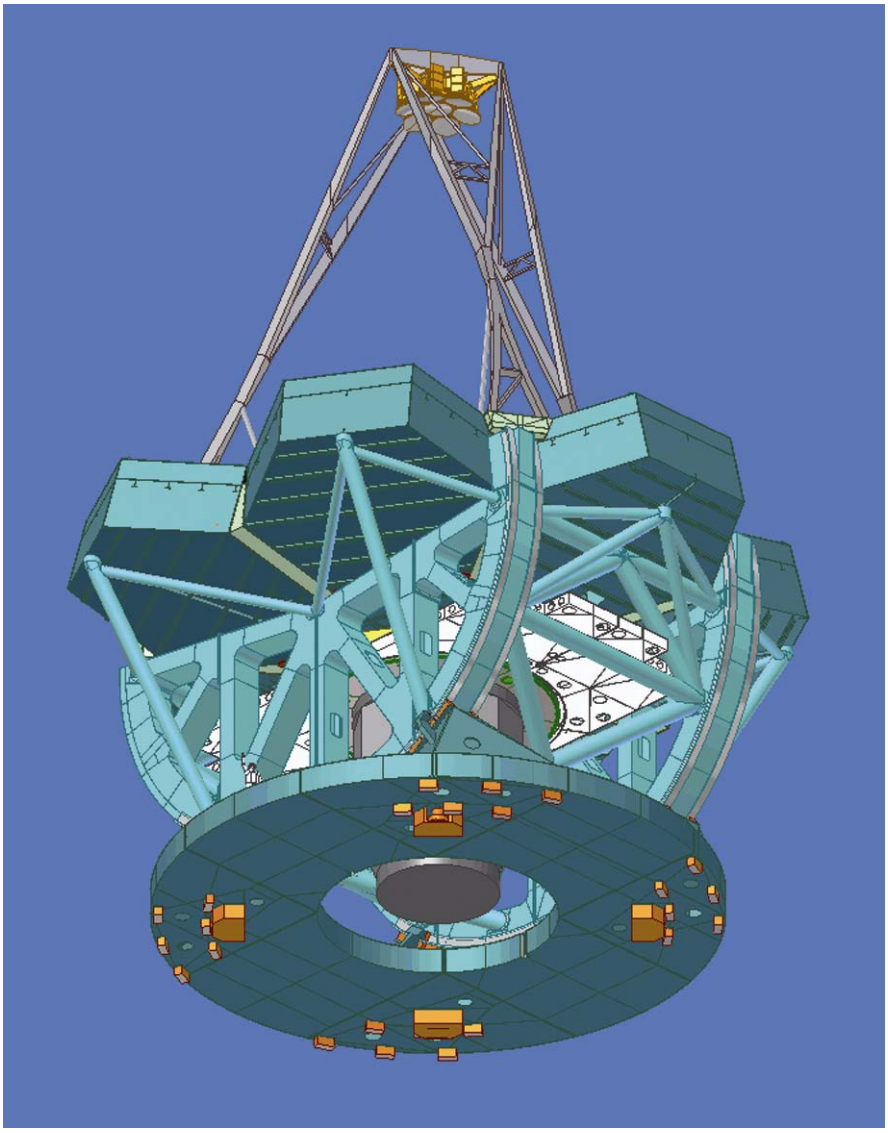

Figure 7-5. Lower view of rotating telescope structure.

7.4.2 C-ring assembly

The c-ring assembly is shown in Figure 7-6. It serves as a base of support for the primary mirror structure assembly and one of the three facets of the secondary truss. It also supports the Instrument Platform. The assembly is made up of two semi-circular structures (c-rings) connected with six sets of K-braces. The machined surfaces on the cylindrical parts of the c-rings are the journals for the hydrostatic bearings that define the altitude axis. Four tripod and two quadrupod brace assemblies mounted to the c-rings provide support for the outboard ends of the six mirror cells. The complete structural assembly weighs 213 metric tons.

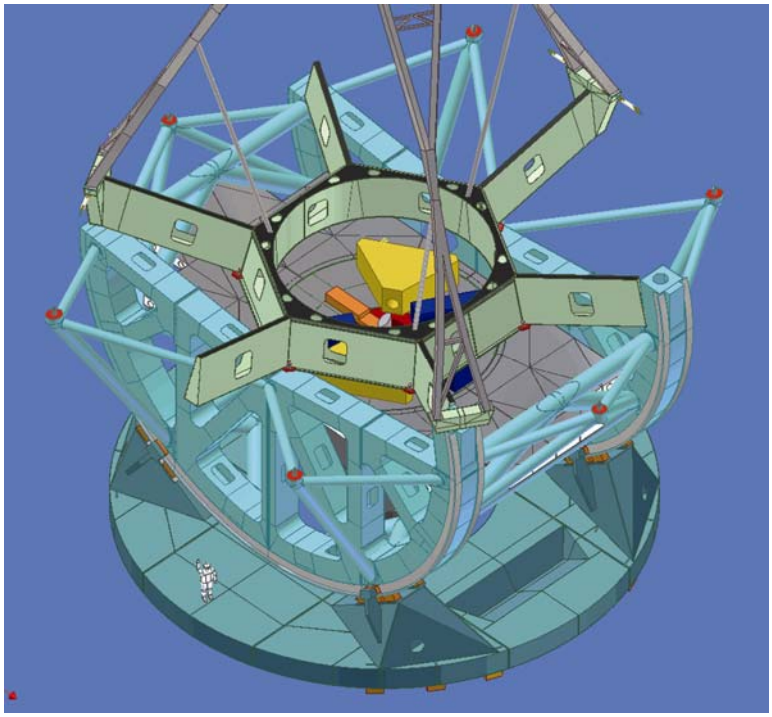

Figure 7-6. Cell Connector Frame, truss, C-ring structure.

7.4.2.1 C-ring structures

For shipping purposes each of the two c-ring structures is made in four main sections plus a front section for extending the bearing surfaces. All sections have precision-machined bolted and doweled interfaces. Each 1.27 meter wide c-ring has two hydrostatic pad bearing surfaces (journals) with an outside radius of 10.4 meters. The c-rings are made predominantly from 12.5 mm and 10 mm mild steel plates with thicker cross-sections locally at manufacturing joints and journals where loads are high (Figure 7-7). The c-rings distribute support forces from the primary mirror structure assembly to the elevation hydrostatic pads and drives. They do this acting globally as space frames and locally as monocoque structures due to large bending and shear stiffness of their box beam sections. Each C-ring weighs 67 metric tons (see Table 7-2).

The extension sections at the front of the c-rings complete the elevation bearing during travel near the minimum elevation angle. One extension serves to stiffly support the bottom of a lower truss assembly using the adapter structure shown in Figure 7-4 and Figure 7-5. The opposite extension must be removed for S3 and S4 cell removal. For this reason and manufacturing commonality, both extensions are being made as separate parts which are not integral with their main c-ring segments.

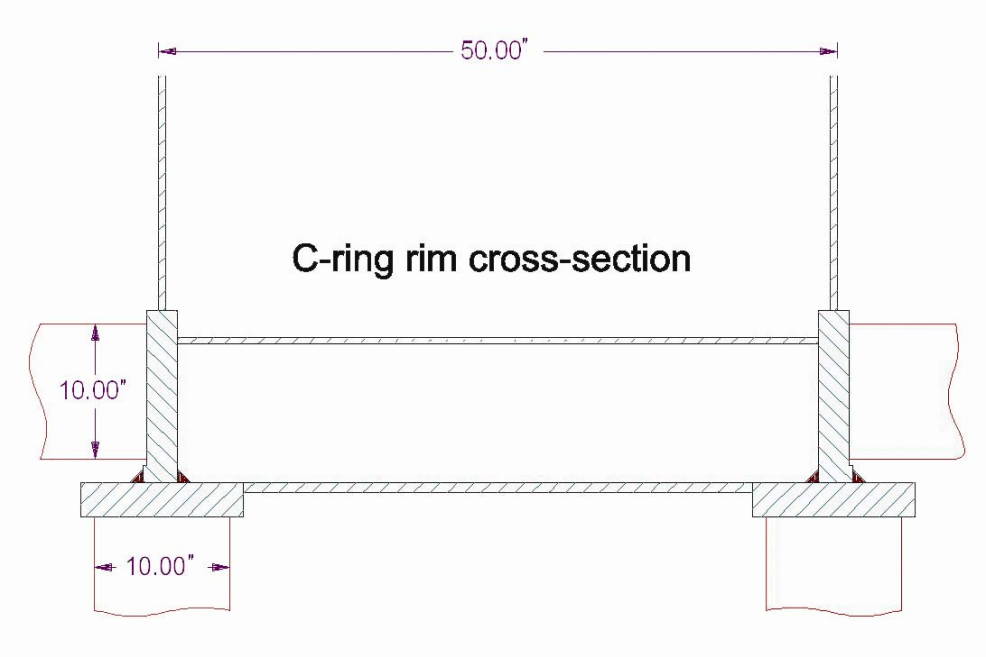

Figure 7-7. C-ring structure.

7.4.2.2 K-braces

The K-braces are the large pipes that connect the two c-rings. The two sets of three braces are symmetric about the lateral central plane through the OSS and act primarily as a space frame, although the bending stiffness from their 760 mm diameter does improve the lowest resonant frequency by approximately 0.4 Hz. A number of alternative bracing systems were analyzed. Although not quite the stiffest, the current design is superior in its accommodation of the IP (see Section 7.4.6 below) and in providing clearance through the structure for the removal of the central mirror cell.

The K-braces will likely be fabricated as complete units. That is, each "K" welded, its end interfaces machined, then shipped as six separate machined weldments. The six K-braces together weigh 53 metric tons.

7.4.2.3 Tripod and quadrupod braces

As shown in Figure 7-6 there are four tripod braces, two mounted on the outer side of each c-ring and two quadrupods braces at the ends of the c-ring structures. These structures mainly serve the purpose of defining the "6^{th} degree of freedom" (dof) for the six outer mirror cells (ref Section 7.4.5.2 below). They only improve the modal performance of the GMT structure slightly, but do measurably stiffen the structure against wind deformations. The braces connect at stiff points on the c-ring structure and thus provide stable defining points for the outer cells. The six braces together weigh 26 metric tons and will likely be made in sections for shipping.

7.4.3 Primary mirror structural assembly

As shown in Figure 7-1 and Figure 7-6, the primary mirror structural assembly consists of the seven mirror cells and a Cell Connector Frame (CCF). The CCF serves to locate and support the seven primary mirror cells and the secondary truss. With all of the elements structurally connected, the assembly acts as a large monocoque structure that contributes significant global stiffness to the OSS. The complete assembly, including cell and CCF structures and the primary mirrors with their support and ventilation systems weighs 420 metric tons. The assembly will be shipped to the site as separate components described below.

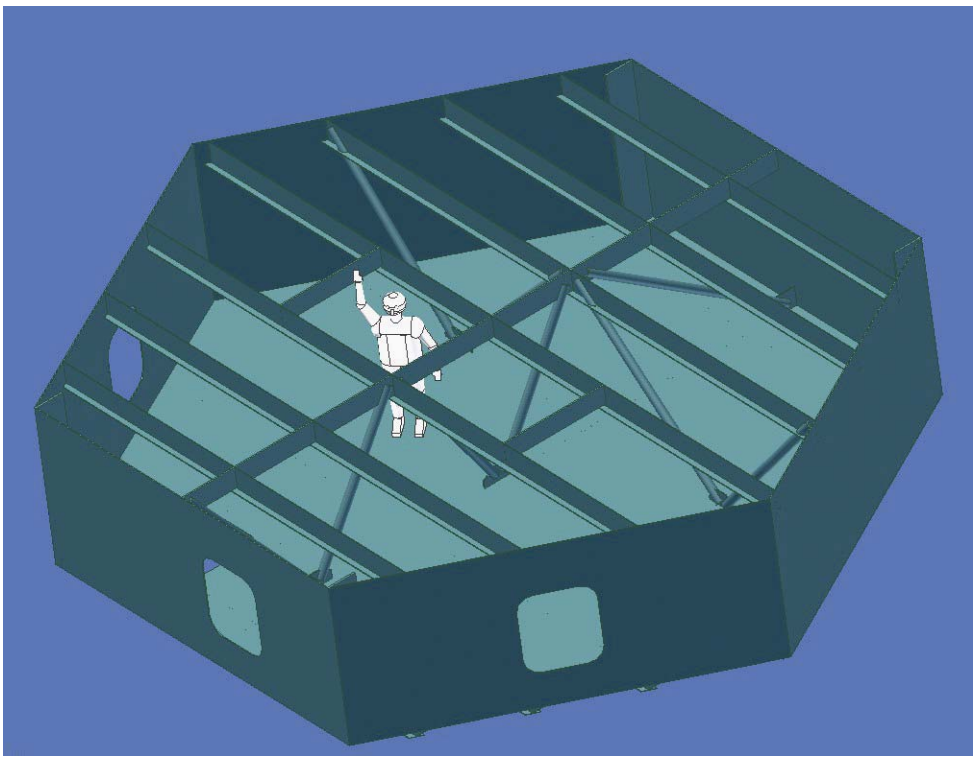

Figure 7-8. Outer cell with top plate and upper structure removed. (Lateral global bracing plane shown here has since been removed from the design.)

7.4.3.1 Primary mirror cells

One outer segment primary mirror cell is shown in Figure 7-8. The solid model view has been cut away with the top removed at a level just below the top plate. The cell structure consists of a top and bottom plate and six outer walls. The mirror support actuators and parts of the mirror ventilation system mount to the underside of the top plate. The supports reach up to the mirror through numerous holes in the plate, see Figure 7-9, photo of LBT cell, for reference. The cells are approximately hexagonal except that the two radial walls are rotated slightly as a result of the 13.52 degree tilt of the outer cells relative to the central cell. (This simple rotation is around an axis perpendicular to the top and bottom plates of the cell). The top and bottom plates are stiffened on their undersides with "T-section" stiffeners to increase local resonant frequencies. The cells are globally braced with one braced plane near the radial central plane of the cell. (The

lateral braced plane shown in Figure 7-8 is no longer required.) An alternative design would eliminate the global bracing but require much deeper and more numerous stiffeners on the underside of the top plate. This is still under consideration.

The cells have been made sufficiently deep to provide reasonable access and comfort to persons working in the cell. The vertical dimension between the bottom and top plates is 2.1 meters. However, with the support and ventilation systems installed, personnel will walk in a stooped attitude when moving around in a cell. In most areas they will be able to stand erect when not in transit. A system of terraced flooring is being considered for the outer cells to improve mobility and comfort. The four 915 mm x 1070 mm access holes in the walls and floor allow personnel to enter or exit at any cell and move between adjacent cells. Although not shown, the center cell is similar in construction except that it is circular, has a large central hole, and radial global bracing.

Figure 7-9. View of top plate of LBT mirror cell. GMT top plate will be similar.

During operation the volume in the cell between the top and bottom plates will be pressurized with conditioned air for the mirror ventilation system. Openings to the outside will be sealed to contain the 85-100 Pa above ambient pressure.

Each of the outer mirror cell assemblies weighs 54 metric tons, the center cell assembly 47 metric tons. The primary mirrors are removed from the telescope in their cells for recoating of the front surface. This is discussed in Section 7.4.5 below.

7.4.3.2 Cell connector frame (CCF)

The CCF is best seen in Figure 7-6. The CCF consists of a central hub and six radial spokes. It is a plate fabrication which serves the purpose of connecting the cells together and maintaining the geometry of the segmented primary mirror. The CCF is attached to the c-ring structure at six points. Although the CCF by itself is not particularly rigid, it becomes part of a very stiff assembly in combination with the seven primary mirror cells.

The central hub has a hexagonal outer shape to interface with the six outer mirror cells with a circular inside diameter to accommodate the round central cell. Approximately 2.1 meters tall, the top and bottom plates of the central hub provide continuous radial load paths in line with the top and bottom plates of the mirror cells cross braced by the sidewalls contributing to the overall stiffness of the assembly. The mirror cell connections to the CCF along the upper flat facets of the central hub define five of the six degrees of freedom for the outer cells (Section 7.4.5.2). The central hub will be made in two sections with precision machined bolted interfaces for ease in manufacture and shipping.

Six radial spokes complete the CCF assembly. These are separate weldments that are bolted to the central hub at precision machined joints. The cells are connected to the spokes at the outer ends with shear plates and braces to control rotation at the spoke ends where the truss attaches. These plus the bolted connection to the central hub constitute the only bolted joints between the CCF and the cells.

Matching doors in the CCF aligned with the access holes in the cells and doors into the CCF from below provide access to inside the mirror cells for service personnel.

The CCF also supports two of the three legs of the secondary truss. (The third truss is supported by one of the c-ring extensions, Figure 7-6).

The CCF will be made in eight machined weldments (six spokes and two central hub halves) and shipped as separate parts. The total assembly weighs 55 metric tons.

7.4.4 Secondary truss

The secondary truss assembly supports the secondary mirror assembly. Considerable effort was expended investigating a wide range of geometries for this structure. Approximately ten fundamentally different trusses were analyzed, a number of them with multiple variations in their geometry and structural properties. Several examples are shown in Figure 7-10.

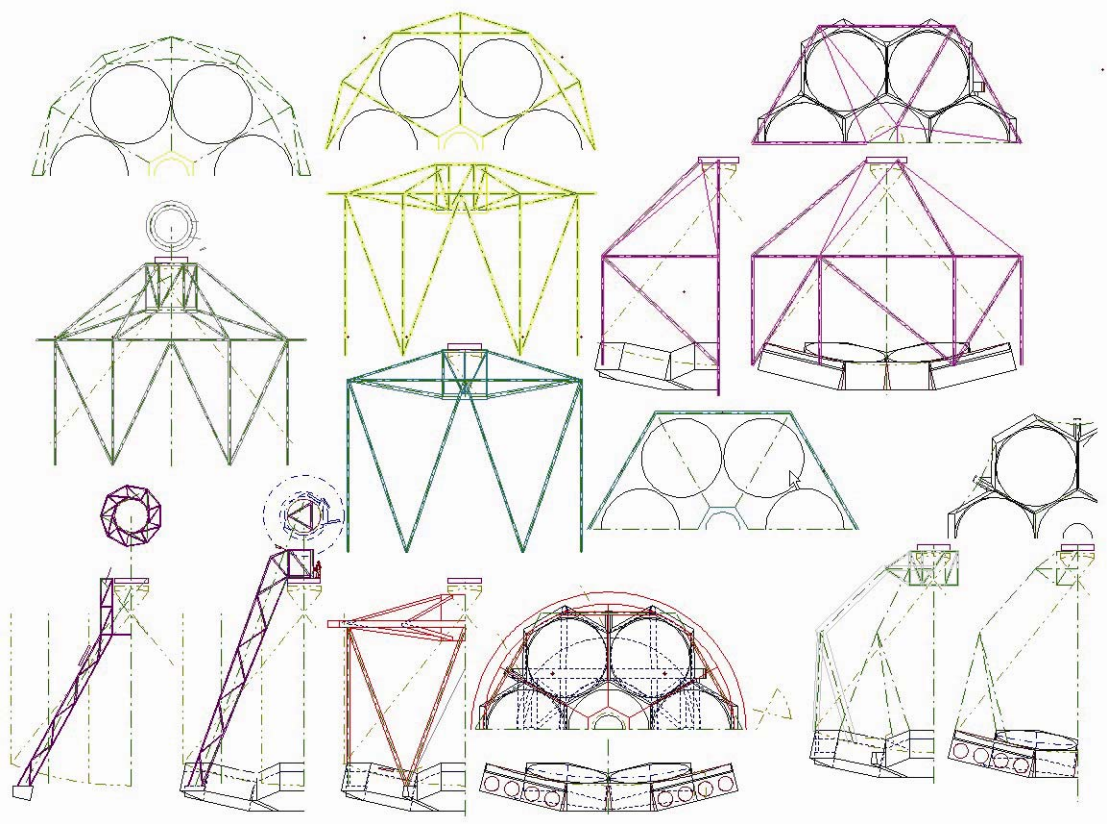

Figure 7-10. Some truss designs considered and analyzed.

7.4.4.1 Truss description

The truss concept finally selected, shown in Figure 7-4, is best described as a braced structural hexapod which stiffly defines all six degrees of freedom for the secondary assembly. By contrast, a tripod or quadrupod defines only the three translational degrees of freedom by truss action and must rely on bending properties to achieve only modest stiffness for the remaining rotational degrees of freedom.

Because of the specific geometry chosen it is not immediately apparent that this is a hexapod. If one defines a structural hexapod as a set of three structural bipods with the bipod nodes separated in space, the bipods here are those three sets of two members with an included angle of approximately 156 degrees when seen in the top view, Figure 7-11. It happens that each bipod member has been connected to a member of the adjacent bipod at the "crossover" point, and the members spread apart using additional bracing below the crossover. Connecting members at the crossover reduces their local vibration spans in the plane that passes through the two members. In addition a crossover brace extends inward and down as shown to reduce the span in the orthogonal plane.

Compared to the other concepts studied, the braced hexapod truss was found superior due to its

low wind area, excellent modal performance, minimal light blockage, reduced diffraction effects, and low thermal mass. As seen in the axial view (Figure 7-11) some of these advantages are specific to the large-segment, unfilled-aperture GMT design. For example, most of the truss silhouette falls in the optically unfilled space between the outer mirror segments. Also, the crossover brace can be attached to the CCF and also reside outside of the light path.

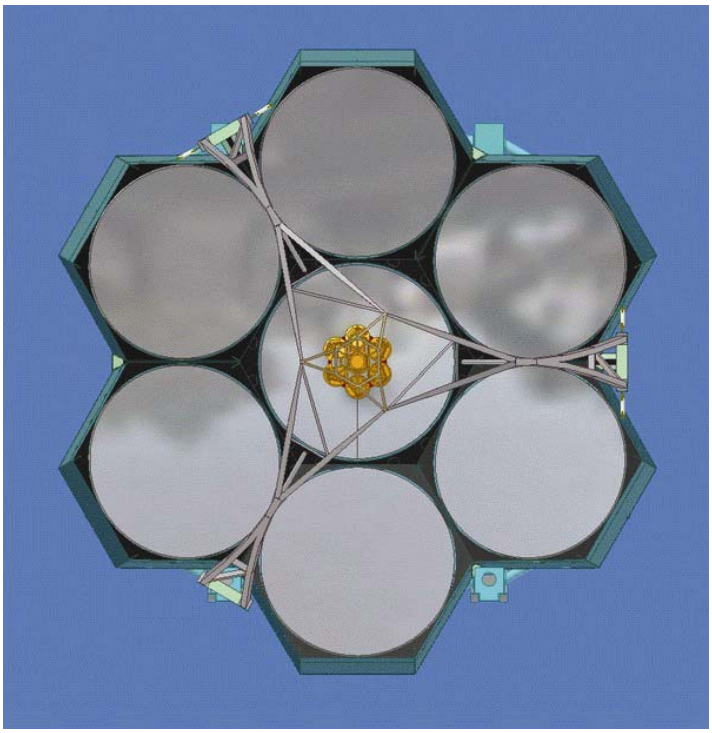

Figure 7-11. Top view of telescope structure.

Due to GMT's fast f/0.7 primary focal ratio the truss members are sufficiently short to achieve acceptable local resonant frequencies with only the bracing described above. Therefore a single-tier truss can be used eliminating the need for a lower truss outside the global light path supporting an upper truss which would transition radially inward to the secondary.

Finally the truss takes advantage of the segmented pupil to put the truss support points on a relatively small radius from the optic axis with two of the three directly over the stiff c-ring structure.

The truss is made of steel below the crossover and carbon fiber reinforced plastic (CFRP) above that point. The use of CFRP is appropriate for this application because of its high mass-specific stiffness and the fact that local resonances contribute measurably to the total truss performance.

7.4.4.2 Recent truss optimization

Although the truss has not yet been fully optimized, recent modal and dynamic response analyses have resulted in physical changes to the truss which have improved performance considerably. The recent changes were:

The secondary support frame was changed from a modified hexagonal shape to the current "faceted triangular" shape. This raised the lowest resonant frequencies for two reasons. 1. It reduced the vertical eccentricity (zenith-pointing reference) from the secondary mass to the effective hexapod support plane as defined by the three bipod nodes. 2. It increased the lateral separation of the three bipod nodes, defining larger moment stiffness.

The support of the lower ends of the truss was stiffened by adding "CCF braces" as shown in Figure 7-12. This reduced the rotation of the lower ends of the truss for modes in which such rotation was significant. Although it had negligible effect on the lowest ("first fundamental") mode frequencies, it increased the second mode frequencies, which reduced line-of-sight (LOS) jitter and image blurring due to wind induced vibration of the upper structure (reference section 7.6.3 below). The braces attach to the CCF and cell with bolted shear connections. This results in zero backlash during use but allows for easy disengagement when a cell is removed for segment recoating.

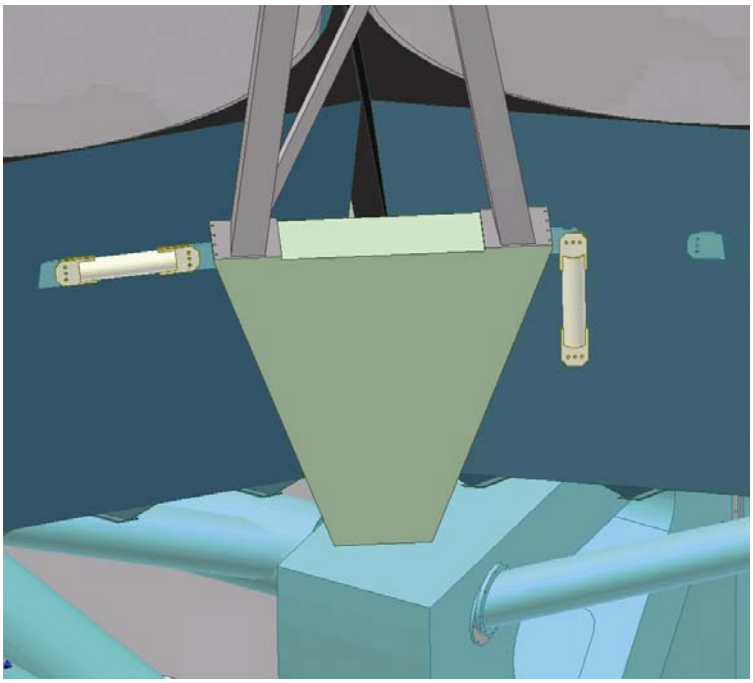

Figure 7-12. CCF braces (left, connected to S1 cell-right, ready for S6 cell removal).

The upper truss area was diagonally braced as shown in Figure 7-4 through Figure 7-6. Although this actually reduced the first translational mode frequencies slightly it significantly increased the second mode frequencies and dramatically reduced LOS jitter. Since these braces are in the incoming light path they do block some light (about 0.3%) but their geometry defines that they will contribute minimally to diffraction.

Finally, the truss main member wall thicknesses were increased. This also reduced the first mode frequencies slightly but resulted in a moderate improvement in the second mode frequencies and reduced wind shake. Detailed results of the dynamic response analyses are presented in section 7.6.3 below.

The current truss design has been fairly well optimized, but some additional performance gains will likely be realized in the next design phase. Optimizations being considered are further lowering of the bipod node geometry, elimination of the intermediate M2 frame and further adjustment of section properties and materials. The current truss consists of 8 metric tons steel and about 7.3 metric tons CFRP.

7.4.5 Cell removal and installation for recoating

The primary mirror cell assemblies will be removed from the telescope for mirror segment recoating. Recoating will take place in a large vacuum chamber in the nearby coating facility at the telescope site. The outer cells are interchangeable in the telescope. There will be a complete spare outer mirror and cell assembly that will be exchanged when one of the other cells is removed from the telescope for mirror recoating. The goal is for the cell exchange to take place in one day to minimize the loss of observing time to a single night. The center segment and cell will not have a spare, thus observations will be interrupted every one or two years for the 1-2 week period required to recoat that mirror.

7.4.5.1 Center segment mirror cell

The center cell will be removed vertically downward by a large equipment elevator that resides in the pier below the telescope (reference section 14.8.1, Central Lift, below). The Instrument Rotator (section 7.7.3 below) is first removed using the same lift, leaving an 8.9 meter diameter hole through which the cell will pass. The cell is defined and structurally connected to the CCF with a precision-machined flange at the top plate of the cell. In addition there is a flexured flange at the bottom of the cell which becomes an additional structural (although not defining) connection to the CCF.

7.4.5.2 Outer segment mirror cells

The outer segments will be removed and installed with an overhead crane with the OSS zenith pointing. As seen in Figure 7-11 the truss support spokes of the CCF prohibit removing the cells along a radial line that passes through the center of the subject cell. Therefore, each cell is removed in a direction parallel to the adjacent CCF spoke with no truss support. With the OSS oriented as shown in Figure 7-11 this simply means that the CCF spoke (not the cell) is aligned with the enclosure centerline while the cell is moved radially toward or away from the telescope. The direction of travel is still consistent with the crane's bridge travel. After removal the cell is moved laterally back to the enclosure centerline using the crane's hoist longitudinal travel and then lowered through a hatch in the observing floor for subsequent processing. The crane will consist of two hoists using 2 two-legged slings or two spreader beams to maintain stability of cell rotation about a vertical axis.

The outer cell registration and connection can best be described using Figure 7-5 and Figure 7-1. Each cell will have five of its six degrees of freedom defined along the interface at the top flat facet of the CCF. The accuracy of this interface will be assured either by precision machining of the interface area of both the CCF and the cell, or by adjusting the interface areas of the CCF to accurate precision using laser metrology methods during the first assembly. The sixth degree of freedom (rotation around a horizontal axis that is parallel to the interface flat) is accomplished by the tripod braces below the side cells and the quadrupod braces below the front and back cells. The large pins on top of the tripods and quadrupods together with the pins at the spoke/hub intersections serve to guide the cell roughly into place as it is lowered the final 300 mm. The pins have sufficient clearance that they only constrain the cell in the vertical direction where they engage. The final positioning is made as the bolts are secured at the CCF hub flat and tripod/quadrupod vertical support. The structural connection of each outer cell will be via approximately twelve 20 mm socket head cap screws at the top and bottom flanges at the CCF hub interface, twelve at each CCF spoke interface and two at the tripod/quadrupod vertical support (50 total).

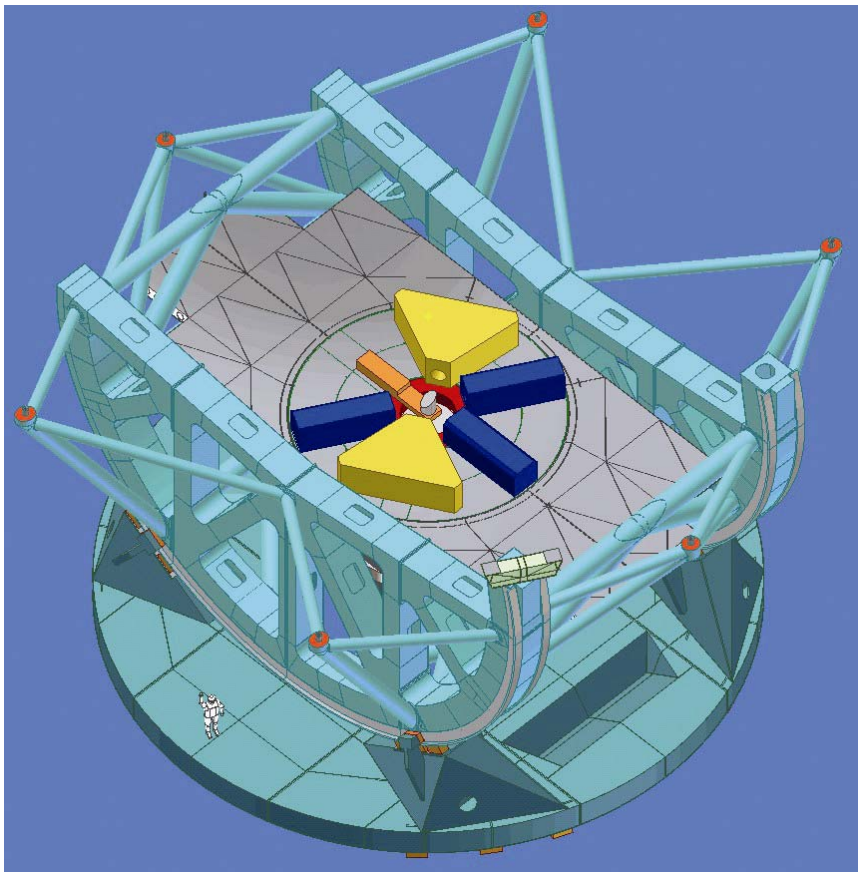

Figure 7-13. Instrument Platform (IP) and Instrument Rotator from above.

7.4.6 Instrument Platform

The Instrument Platform assembly is shown in Figure 7-13 and Figure 7-14. It consists of a stationary Instrument Platform (IP) that is 10 meters wide by 20.4 meters long with an 8.84 meter diameter rotating platform (Instrument Rotator) at its center. Mounted in the center of the Instrument Rotator will be the wavefront sensor probes for the active optics system. As shown the Instrument Rotator accommodates large Gregorian instruments below (up to 6.4 meters dia. by 7.6 meters long, weighing 23 metric tons) and up to six small to medium size folded-beam instruments above with average weights of 1,800 kg. In addition, the system can be used without rotation to feed other large stationary instruments mounted on the IP. It is tentatively planned that the multi-conjugate adaptive optics (MCAO) instrument will be mounted in this way. Such instruments would require their own guiding and focus assemblies.

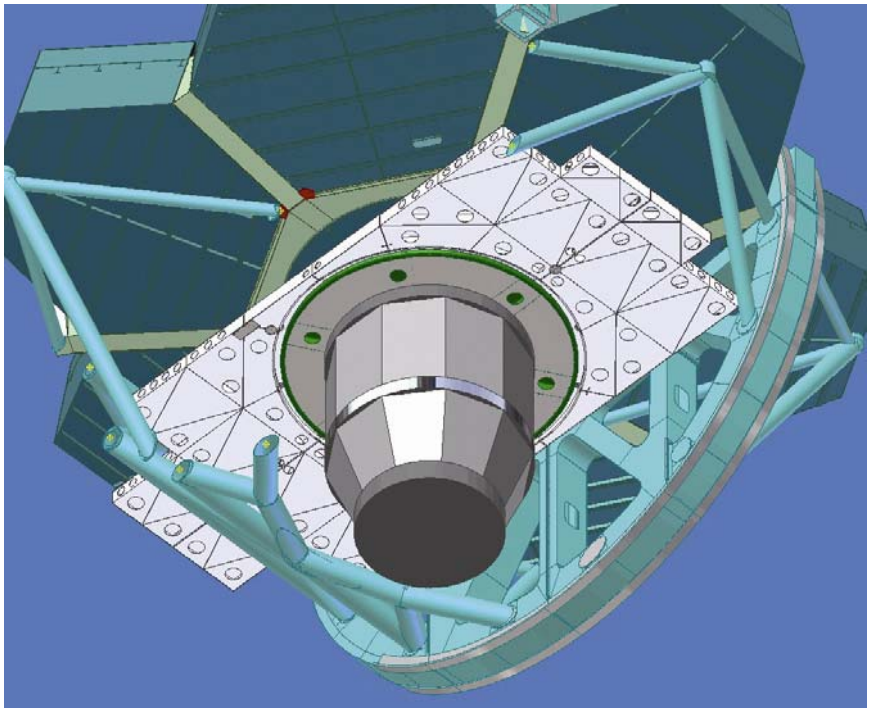

Figure 7-14. IP and Rotator from below (C-ring and some braces removed for clarity).

The large Gregorian instruments will be installed and removed using the central lift. These exchanges will be done during the day. Multiple smaller instruments may be packaged in a single Gregorian instrument module to increase the flexibility of the instrument configuration. Exchanges between these smaller instruments and between the folded beam instruments on the top side can be done during the night. The folded instruments are loaded and off-loaded to the top side of the platform with a lift which brings them up from the observing floor. This is done at the back end of the platform through the opening in the rear K-braces.

The IP and Instrument Rotator have a combined weight of 43 metric tons. The complete assembly with instruments and mechanical systems weighs 80 metric tons. A more detailed discussion of the Instrument Platform is included in section 7.7.3 below.

7.4.7 Azimuth structure

The azimuth structure is best seen in Figure 7-15 and Figure 7-16. It consists of two major structural features: the large diameter, vertically thin azimuth disk and four compact, robust OSS support pedestals.

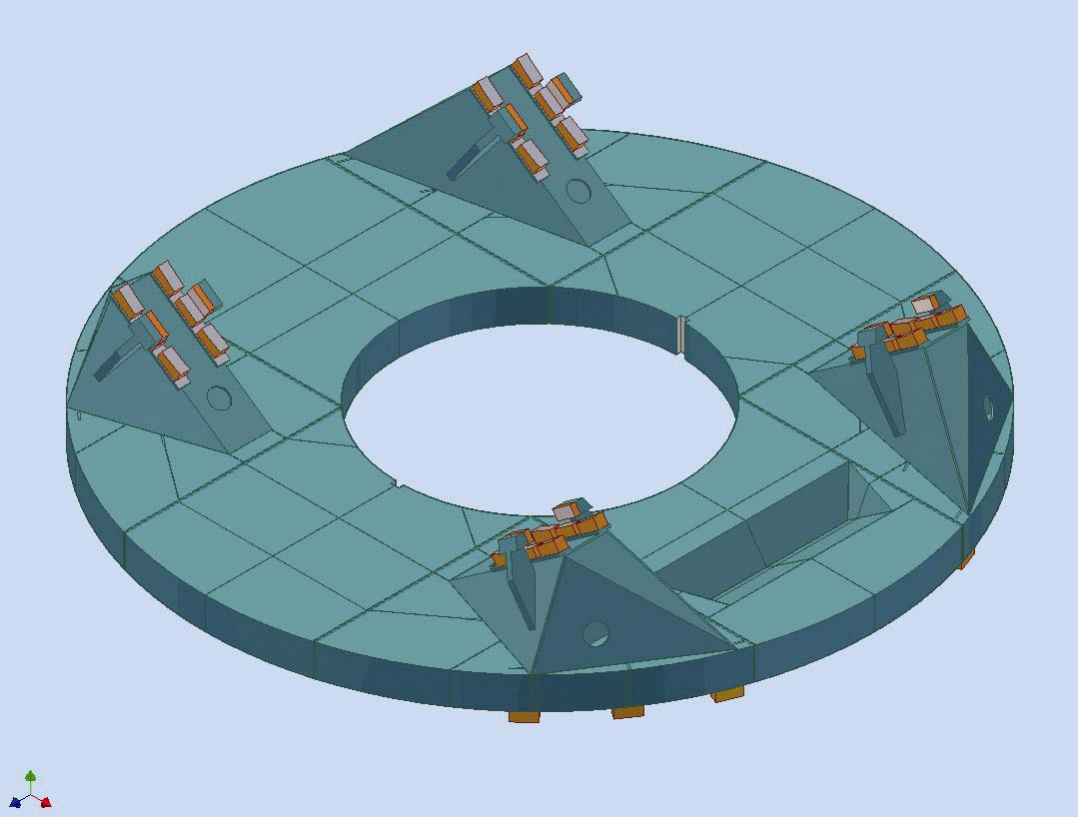

Figure 7-15. Upper view of azimuth structure. Visible are OSS radial and lateral hydrostatic pads, OSS support pedestals, S4 cell minimum elevation clearance recess, and central lift guide notches.

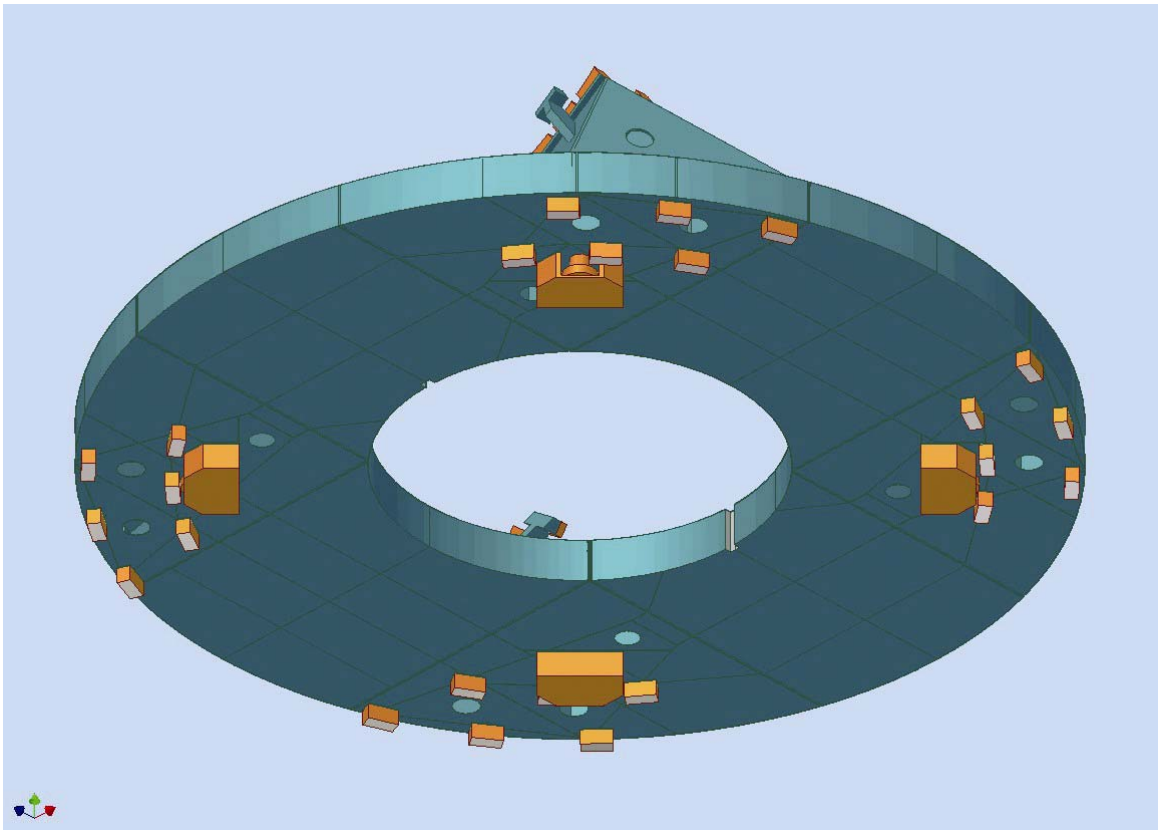

Figure 7-16. Lower view of azimuth structure. Visible are azimuth vertical hydrostatic pads and lateral defining and drive rollers.

7.4.7.1 Azimuth disk

The azimuth disk has a 21.3 meter outside diameter with an 8.9 meter diameter central hole. Its vertical thickness is 1 meter. It will likely be made in eight sections with precision machined bolted interfaces. It is constructed predominantly from 12.5 mm steel top and bottom plates and has numerous internal reinforcements. The front area of the disk includes a reinforced notch through most of its vertical thickness to clear the front center mirror cell when the OSS is commanded to its minimum elevation angle, currently 28 degrees. The project goal is to achieve 25 degrees in the next design phase. The azimuth disk serves to transfer global support of the OSS to the stationary azimuth track and pier below as well as providing a work surface to enable convenient access to drives, hydrostatic bearings and other equipment. The central hole in the azimuth disk will be filled with a non-structural platform installed by the central lift.

7.4.7.2 OSS support pedestals

The four OSS support pedestals serve to transfer the local vertical and horizontal loads from the OSS through the azimuth disk to the azimuth track below. The elevation and azimuth hydrostatic bearings and azimuth rollers transfer the loads at the interfaces. Each of the four OSS support pedestals is defined to the azimuth track with three master hydrostatic pads and three slave pads with high frequency over-constraint (HFOC). HFOC, described later in section

7.7.1, provides stiff support for high frequency disturbances but allows the bearing to adjust its height to accommodate manufacturing variations and flexure in the structure, which are slow, or low frequency effects.

The pedestals have six radial pads on their top side with lines of action to the altitude axis with an average force angle of 35 degrees from vertical. The average line of action of these forces intersects the average line of action of force for the six vertical pads to the azimuth track in a plane that lies within the azimuth disk. There is a horizontal component of force where these vector forces sum that is reacted directly by in-plane membrane stresses in the azimuth disk with no bending moment. Lateral forces and stiffness in supporting the OSS are by two lateral pads at each pedestal. Due to the significant vertical height from that level to the azimuth track, lateral stiffness from the pedestals relies on moment stiffness from the pattern of six vertical hydrostatic pads below. This is achieved by differential forces in the vertical pads to the azimuth track which in turn transfers moments to the pier immediately below.

7.4.7.3 Radial and tangential definition

The horizontal definition of the azimuth disk (and therefore the telescope) is to the inside radius of the top flange of the azimuth track. The radial definition is done with four 760 mm diameter precision rollers mounted on the underside of the azimuth disk with 90 degree spacing around the azimuth axis. Two adjacent rollers are rigidly defined to the disk, the two opposing rollers are modestly preloaded with HFOC to provide a constant preload for the azimuth drives. Rotation of the telescope about the azimuth axis is accomplished using four gear or friction drives acting through the rollers.

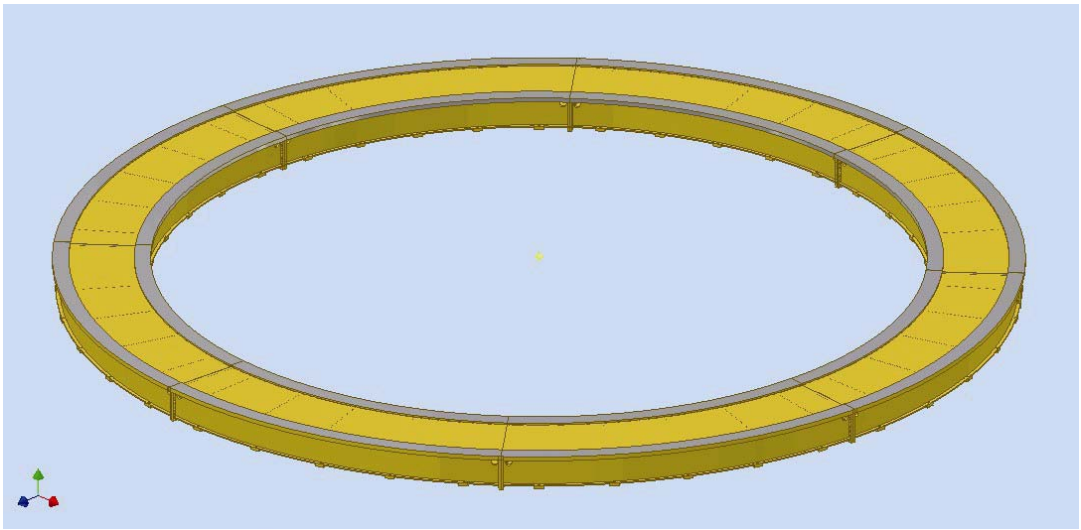

Figure 7-17. Upper view of azimuth track with machined hydrostatic runner bearings and roller interface surface at upper inside diameter.

7.4.7.4 Azimuth track

The stationary azimuth track stiffly and precisely couples the telescope to the pier as shown in Figure 7-3. It is made of steel and considered part of the telescope structure. A shallow box beam structure, it is made in 8 or 9 sections which are bolted and doweled together, Figure 7-18. The precision machined top bearing surface and inner diameter roller running surface on the top flange will be adjusted and locally finished on-site to have acceptably small steps at the manufacturing joints. The proper functioning of the hydrostatic bearings requires that the steps at the hydrostatic bearing surfaces are less than 10 microns. Steps in the roller running surface are somewhat less critical. After the sections are bolted and doweled, the assembly will be adjusted flat using 52 adjustable anchor fittings. Circularity will be achieved using horizontal screw jacks.

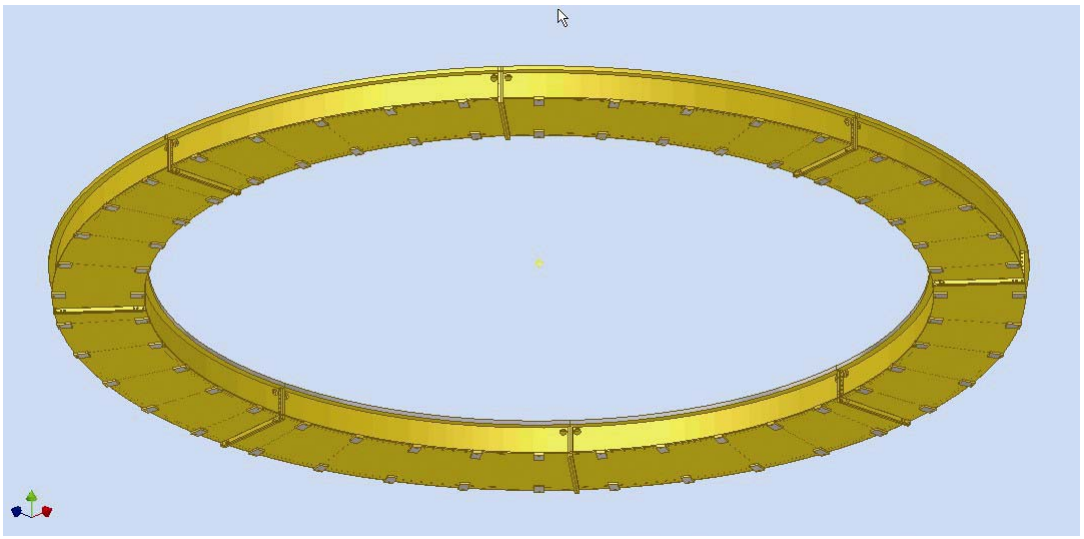

Figure 7-18. Lower view of azimuth track. Visible are manufacturing joints and machined pads which interface to adjustable anchors to pier.

The 52 anchor point geometry was selected to match the spacing of the vertical hydrostatic pads under the four pedestals so that when any pad is directly over an anchor point the other 23 pads are also over anchor points (the minimum track defection condition) and when any pad is midway between anchor points (the maximum track deflection condition) so are the other 23. The synchronized geometry is shown in Figure 7-19. (Figure 7-17 and Figure 7-18 show an older spacing). The result is that the pedestals translate vertically in phase as the telescope rotates in azimuth and to first-order neither the pedestals nor the telescope tilt due to azimuth rotation. This will simplify the pointing model for the telescope control system and likely improve pointing accuracy.

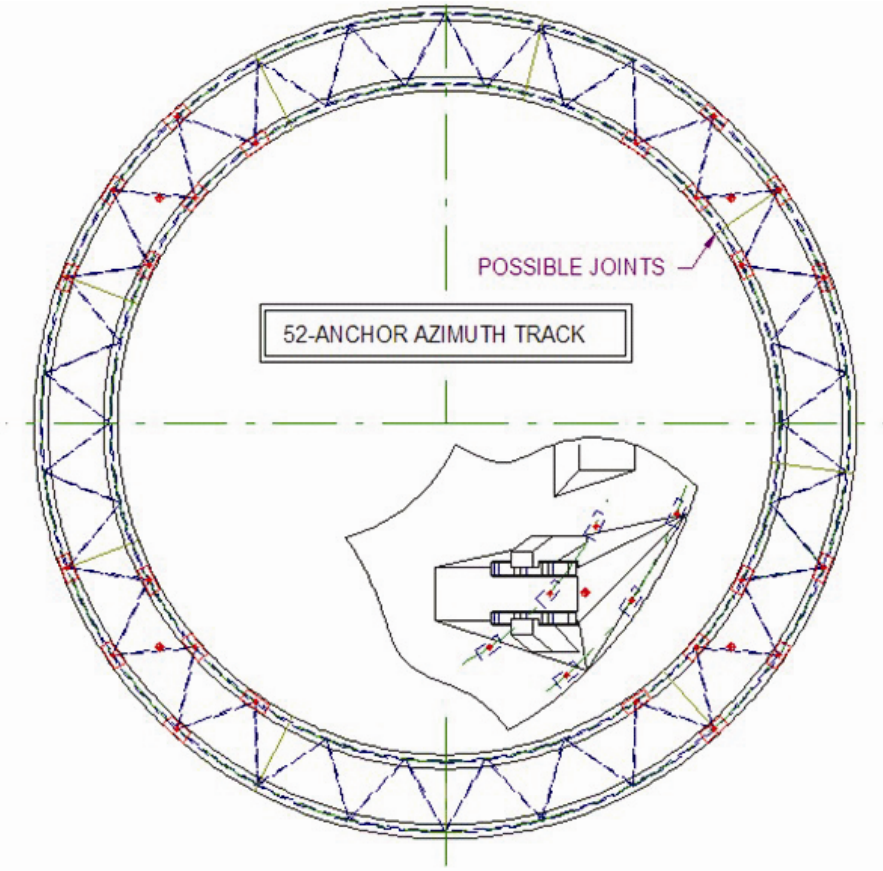

Figure 7-19. Synchronized azimuth track support pad and azimuth hydrostatic pad geometries.

In addition to the periodic small vertical translation due to bending and shear in the azimuth track, there will be a nominal 90 micron constant vertical deflection from the pier when pedestals are over the solid areas of the pier. This increases to about 150 microns when a pedestal is over the center of a portal. However, since the portals and pedestals have 180 degree symmetry, and with the low vertical bending stiffness of the azimuth disk, the net effect of the portals is to produce a sinusoidal lowering and raising of the telescope by (150 - 90)/2 = 30 microns with a 90° period in azimuth rotation. This is a negligible effect.

7.4.8 Cost Estimate Structure Drawings

A significant effort has been the creation of a set of drawings of the telescope structure to be used for the concept design cost estimate. This process involved revision of the solid model part files to incorporate much more detail, followed by the creation of the 2D CAD drawing files of each major machined weldment. This was done for all major structural parts except the secondary truss and M2 frame.

Graphic views of a typical part (the 00015 Azimuth Disk Pedestal Segment) are shown below. (Figure 7-20 and Figure 7-21). Although not discernable at this scale, the 2D drawings have adequate detail to convey all structural features, basic dimensions, plate thicknesses, welding and stress relief requirements, machining requirements, and an accurate weight for each part (Figure 7-22).

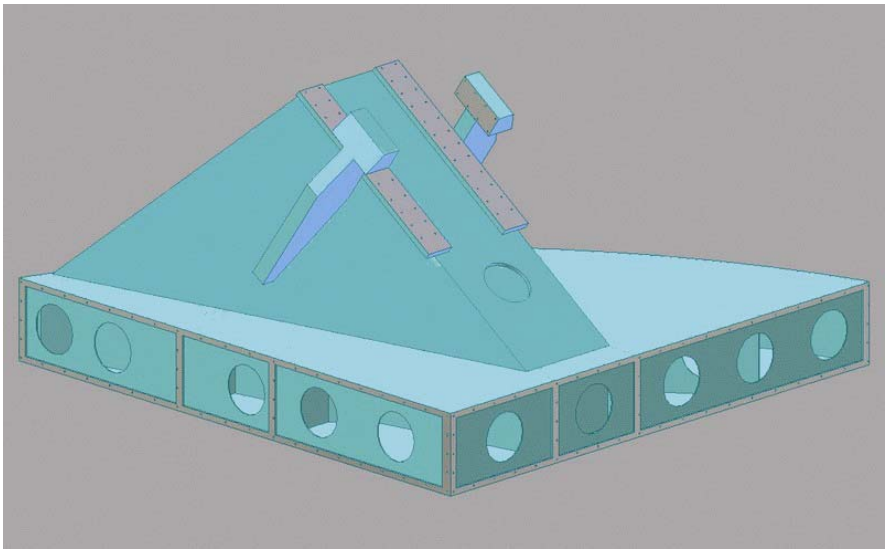

Figure 7-20. Upper inner view.

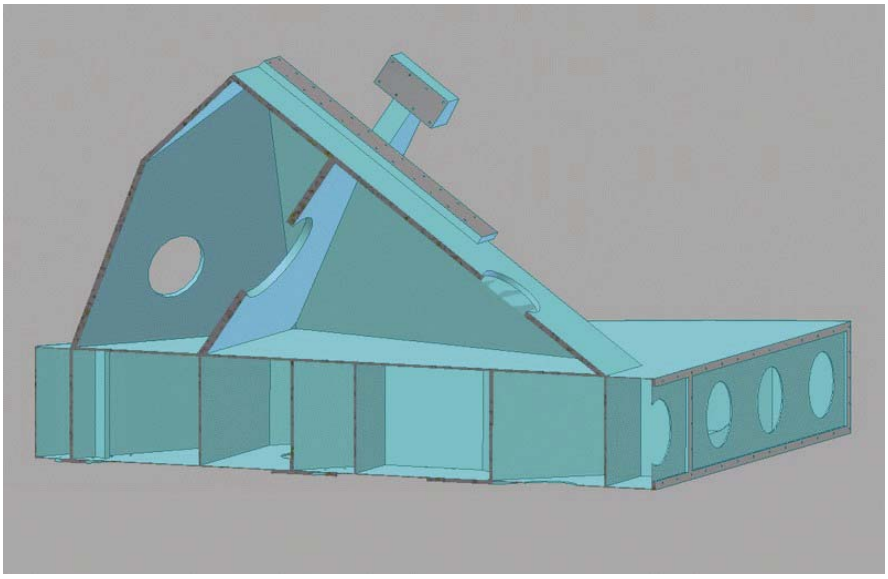

Figure 7-21. Vertical sectional view.

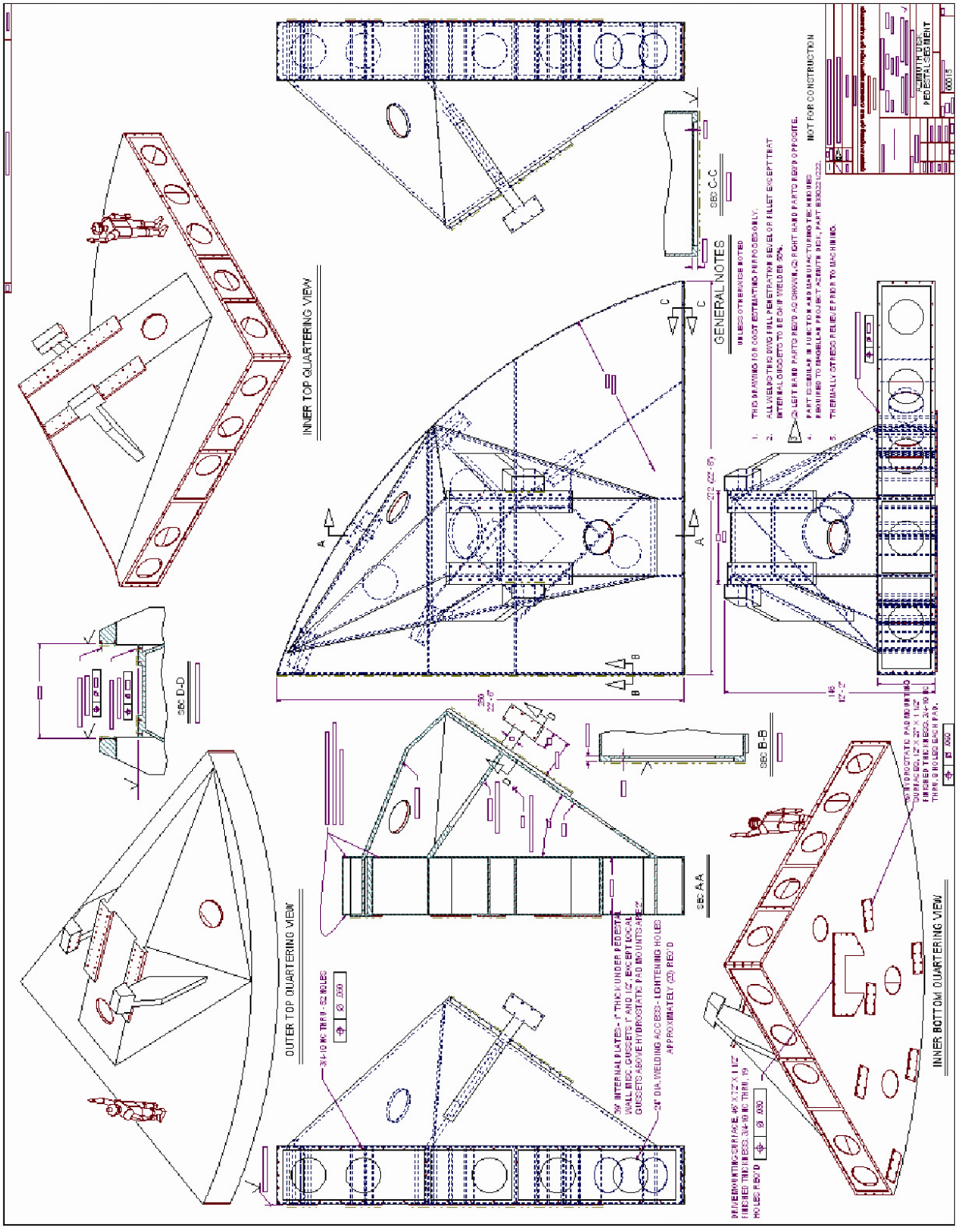

Figure 7-22. 2D CAD drawing, 00015 Azimuth Disk Pedestal Segment. Typical drawing used for cost estimate by manufacturers.

7.4.9 Weight summary

A summary of the telescope rotating and total weights of the GMT follows:

Table 7-2. GMT Weight Summary.

Description	Detail	Weight Metric tons	Total Metric tons
Secondary assembly	structure (steel) optics & mechanical	2.3 4.1	6.4
Secondary truss	steel CFRP	8.2 7.3	15.5
CCF (cell connector frame)	steel	55	55
Primary cell assembly (7)	steel glass mechanical	213 113 40	366
C-ring assembly	c-ring structures (steel) main braces (steel) tripods/quadrupods (steel)	134 53 26	213
IP assembly	structure (steel) folded instruments (6) Gregorian instrument mechanical	43 11 23 3	80
Total weight OSS Assembly	-	-	**735**
Azimuth assembly	steel drives, hydrostatics, etc.	221 48	**270**
Telescope Rotating Weight	-	-	**1005**
Telescope Non-rotating Weight	azimuth track	(118)	118
Total Telescope Assembly	-	-	**1,123**

7.5 **Pier**

The pier serves to elevate the telescope to accommodate removal of large Gregorian instruments and the center mirror cell, Figure 7-23. The two-step removal process involves lowering an assembly then moving it horizontally through a large opening (portal) in the pier. A second benefit of the pier being tall is that it raises the telescope up with respect to the ground layer, reducing site seeing. The pier must do this and still provide a very stiff transfer of the support of the telescope to ground.

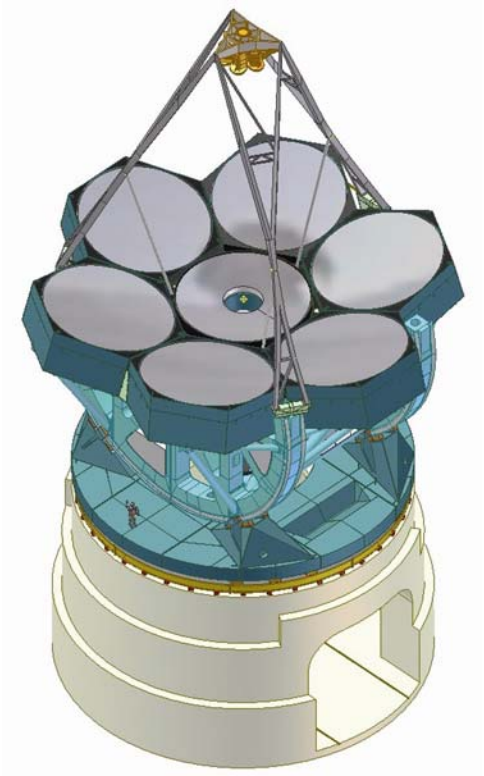

Figure 7-23. GMT and pier structure.

The reinforced concrete structure is shown in Figure 7-24 through Figure 7-26 below. With an outside diameter of 23.8 meters, the pier extends 12.5 meters above grade. It has a maximum wall thickness of 3 meters and at 5,400 metric tons it is much more massive than the telescope, which weighs 1,123 metric tons. Features visible in the figures below are the large top hole for vertical passage (and the large portals for horizontal passage) of the S7 cell, Gregorian instruments, and Instrument Rotator. Also shown are the cart support rails, the central lift pit where the stiffened platform lives when not in use, and the upper area of the hole for the hydraulic lift cylinder. One of two ventilation system inlet holes, which will connect to a below-grade exhaust tunnel, is shown in Figure 7-24 and 7-25. Finally, access to the azimuth hydrostatic bearings, azimuth drives, and the azimuth utility transfer system will be as shown in Figure 7-26.

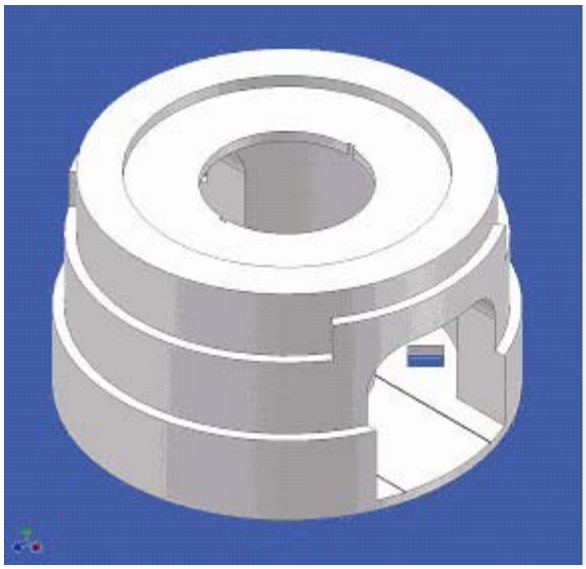

Figure 7-24. Quartering exterior view of pier.

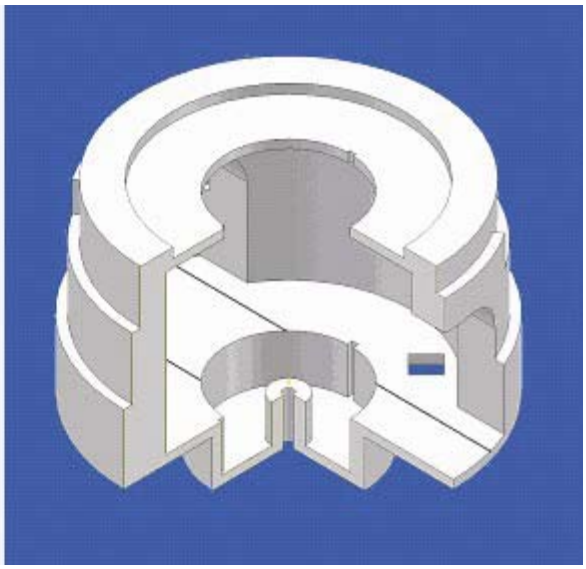

Figure 7-25. Quartering sectional view of pier.

Access to and between those areas will be via stairs and two holes in the pier which are not shown. The outer circular platform will be accessible by an elevator at the mezzanine level.

The design evolved from an initial design which was considerably less stiff, using the following progression:

1. A modal performance goal of 12 Hz. was established for the pier supporting a rigid mass equal to that of the telescope. The mass was applied at the telescope center of gravity but in such a way that it did not stiffen the pier, although the telescope will stiffen the top of the pier somewhat. This goal would assure that the modal performance loss due to pier compliance would be small as compared to the ~5 Hz telescope lowest mode. In this way finely meshed models of the telescope and pier could be used separately without requiring large finely-meshed models of the two structures combined.

2. A baseline design with a 1.8 meter constant wall thickness was analyzed and found to have an unacceptably low first mode frequency of 8.6 Hz.

3. Various optimizations were tried. Increasing the wall thickness (stepped from 3 meters at the bottom to 1.8 meters at the top) increased the 8.6 Hz to 10.6 Hz. Reinforcing the portal sides and upper corners plus including considerable stiffness from the telescope raised the 10.6 Hz to 15.6 Hz. Then reducing the stiffness from the telescope to a more realistic value dropped the frequency to 14.2 Hz. It is noted that all of the models to this point assumed rigid support by the ground below.

4. Finally, the effect of the ground support below was included. From the Magellan geotechnical report (supplied by M3 Engineering and Technology, Inc.) the soil at the Magellan site had a Young's modulus of 3.4E10 Pa. A range in modulus of 1.38E10 Pa to 8.3E10 Pa was used in the analyses to determine the sensitivity to the ground support. These values are representative of rather hard rock, typical at Las Campanas, Chile. A 73 meter diameter x 37 meter deep volume of material was used beneath the pier in a new model. As compared to the rigid-support first frequency of 14.2 Hz, the results were as shown in Table 7-3.

It is estimated that the pier described above, supported by rock typical at Las Campanas, will degrade the first mode frequency of the telescope by about 0.2 to 0.25 Hz.

Table 7-3.

Finite element model GMT104 - GMT103 with soil support below			
Mode - Description	1.4E10 Pa soil Frequencies, Hz	**3.4E10 Pa soil Frequencies, Hz**	8.3E10 Pa soil Frequencies, Hz
1 - Lateral translation	12.1	**13.2**	14.0
2 - Fore-aft translation	12.5	**13.8**	14.5

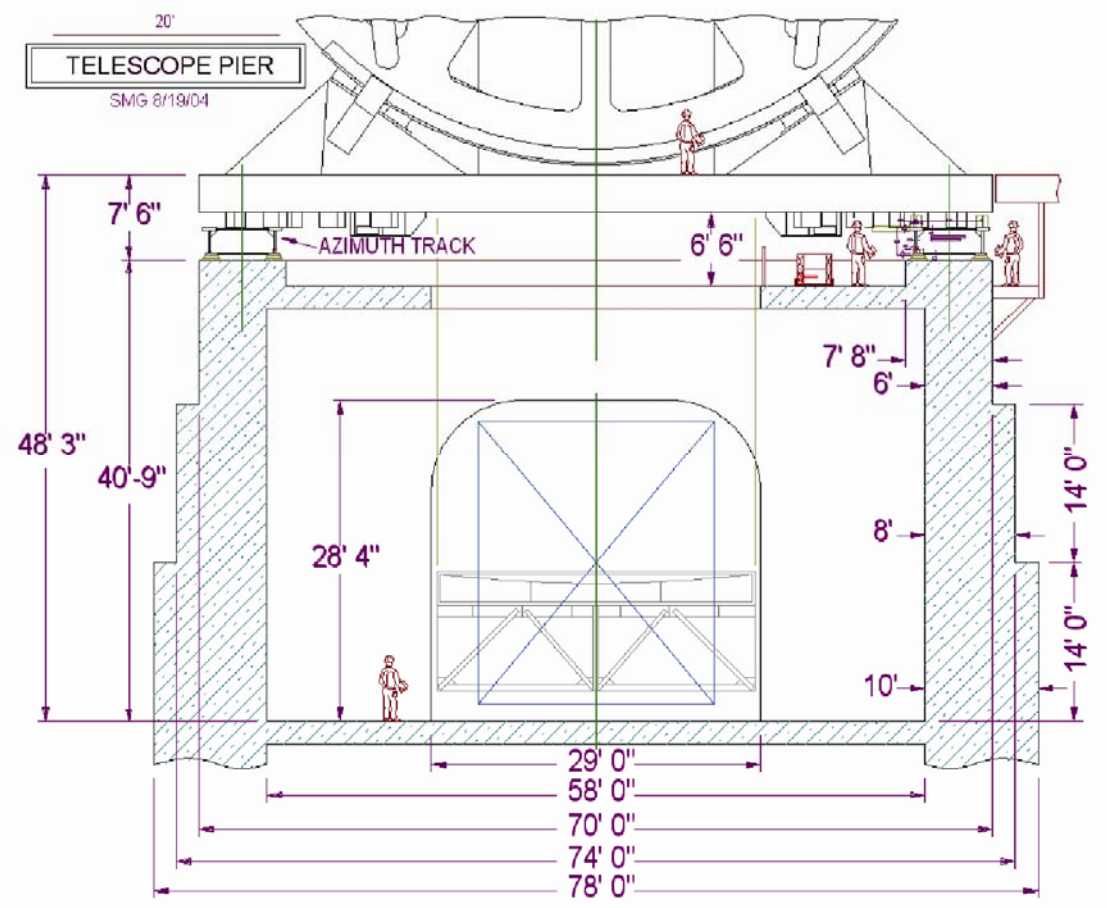

Figure 7-26. Pier dimensions.

7.6 **Performance**

7.6.1 Gravity Deflections

The optics of GMT and instruments in the focal plane will displace relative to each other as the structure rotates in elevation. The active alignment system described in Section 8 will correct for the misalignment by tilting and translating the primary and secondary mirror segments to maintain alignment and focus. The motions may be obtained by applying gravity loading to the GMT FEA model for two elevation angles and noting the change in displacements.

The primary mirror segments are represented in the GMT FE model by plate elements with mass and stiffness properties representative of the average properties of the actual mirrors at their central plane. Each is defined in its cell with hexapod actuators (hardpoints) with the stiffness properties of the hardpoints of the LBT mirror supports. Loadcells between the top of the hardpoints and the mirror measure the forces being applied by the hardpoints. A distributed set of force actuators attached to the mirror act to null out the forces so that the quasi-static displacements at the mirror reflect the self deflection of the hardpoints (small) and the motions at the hardpoint attachments to the cell. (The mirror support system is described in Section 10.3.) Their hardpoint geometry was optimized for a combination of minimum segment motion under gravity loading and maximum local modal performance.

Individual cells are connected to adjoining cells and to the telescope structure through the CCF. Even with kinematic definition of the segments by the hardpoints in their cells, relative motion of the segments results from distortion of the GMT structure including the cells. Since mirror distortion is negligible at the level of the structure's deflection, nodes at the center of each segment provide the virtually rigid body translation and tilt of the segment.

The secondary mirror is represented in the FE model by a lumped (non-segmented) mass connected to the upper truss assembly with a hexapod support. The deflection of the mirror segments relative to each other will be small compared to the gross motion of the truss assembly and motions of the primary segments and is ignored in this model. The motion of the secondary mirror is tracked with a node at the position of the mirror vertex.

The Instrument Platform is tied to the C-ring structure of the telescope and carries the instrument load. A load of 79,500 kg was applied to the platform at the combined center of gravity of the platform and Gregorian and folded-port instruments. Deflections were tracked at the center of the focal surface.

The wide-field corrector and ADC are tied to the center primary mirror cell and will follow its motion.

Table 7-4. Optics deflections relative to S7 reference plane, ZD = 0 -> 56.6824 degrees.

	x txl microns	**y txl** microns	**z txl** microns	**x tilt** microrad	**y tilt** microrad	**z tilt** microrad
S1 vertex	29.1	-174.6	-32.5	23.1	12.8	4.5
S2 vertex	103.8	-23.7	-150.1	-24.4	22.8	-14.3
S3 vertex	48.0	76.9	9.6	-21.7	31.3	-21.0
S4 vertex	-14.8	-49.3	42.7	54.7	-0.7	0.5
S5 vertex	-102.4	83.3	-28.4	-22.1	-44.0	23.9
S6 vertex	-99.7	-71.6	-135.8	-0.9	-28.0	10.8
S7 (center mirror) vertex	0.0	0.0	0.0	0.0	0.0	0.0
M2 vertex	41.5	-3451.5	220.2	-318.0	-10.5	29.5
Instrument Platform	7.2	38.0	-223.0	-101.9	2.9	-0.4

Table 7-4 shows the deflections of the GMT primary mirror segments, secondary mirror, and Instrument Platform with respect to the central primary mirror segment, S7, when the telescope moves from zenith pointing to a zenith angle of 56.7°, the lowest angle for which the model is valid (GMT Document 1087). Primary mirror segment S1 is at the top with the telescope pointed at horizon and S2-S6 are numbered consecutively clockwise as viewed from the secondary mirror. The x-axis is parallel to the elevation axis, the z-axis is along the optical axis and points up when the telescope is at zenith, and the y-axis is perpendicular to x- and z- and points up with the telescope pointing at the horizon.

The maximum hardpoint actuator travel required to accommodate the worst case combination of segment gravity piston and tilt in the above table is 0.29 mm p-v across the full back surface of the mirror segments. This does not include the deflection of the top plate of the cell upon which the support actuators are mounted. An additional 1.5 mm p-v of actuator travel is required for this effect. The hardpoints are stiffly supported at the intersection of the cell bottom plate and outer walls and do not deflect with the top plate except to the extent that the top and bottom plates are structurally tied together. This is included in the deflection numbers above.

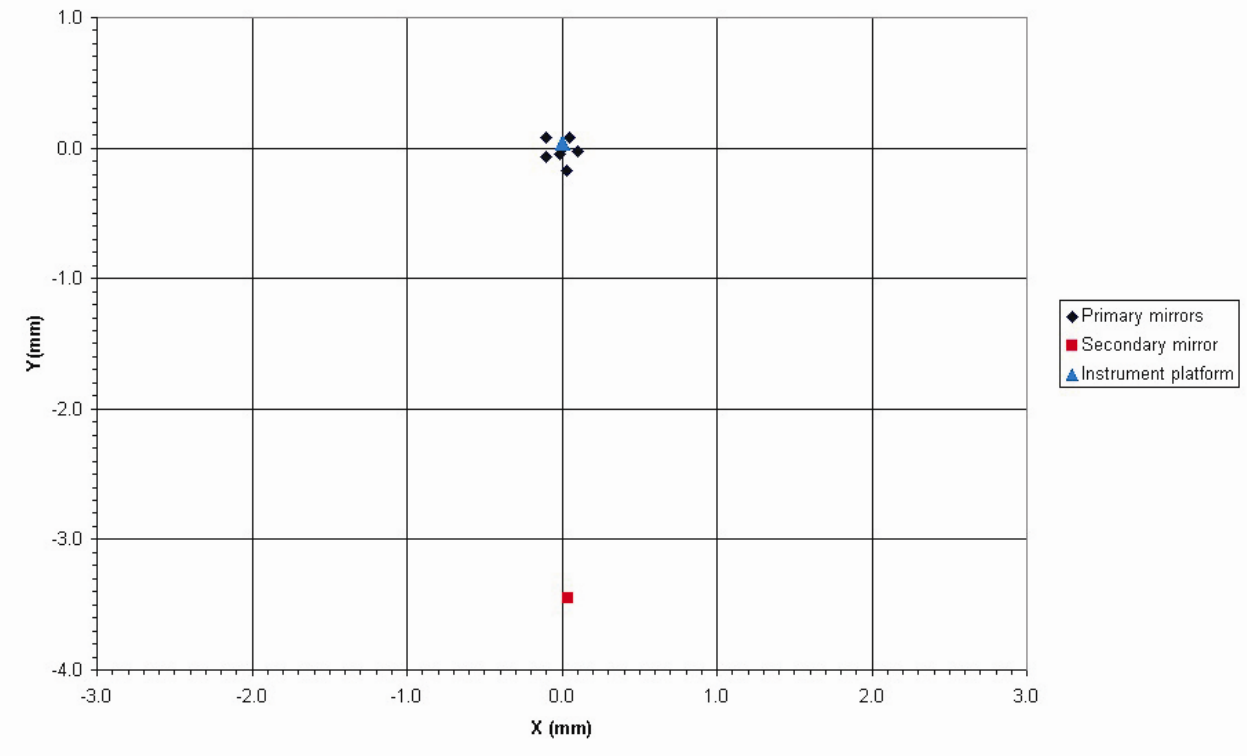

Figure 7-27. X-Y deflection of the GMT optical surfaces relative to the center primary mirror segment from the zenith to zenith angle 56.7°.

The secondary mirror assembly experiences the greatest motion due to sagging of the upper truss as shown in Figure 7-27. The motions of the primary mirror segments, although small, will also require active correction.

7.6.2 Modal Performance

Finite element analysis has been used to calculate the natural frequencies and mode shapes for the telescope structure. Many optimizing runs were made to understand performance-critical properties of the structure with the ultimate goal of maximizing the fundamental mode frequencies. (The lowest frequency modes in which all telescope mass vibrates in phase – see 7.6.2.2 below).

A typical telescope finite element model is shown in Figure 7-28. The first three mode shapes were consistently found to be (in order) lateral translation, fore-aft translation, and azimuth rotation as shown in Figure 7-29 through Figure 7-31.

7.6.2.1 FEA Summary

Approximately 40 truss local models and well over 100 complete telescope models have been created and solved during the design process thus far. Detailed results are summarized in various

informal project engineering reports GMT1.pdf through GMT29.pdf. Some examples of a few of the studies and optimizations are:

1. Widely varying geometries were analyzed for the secondary truss. The result was the braced hexapod truss seen throughout this report. Its features and advantages, as well as recent optimizations, are discussed in section 7.4.4 above.

2. Modal performance gain as a function of high frequency over-constraint (HFOC). An early telescope design model was run with modest overconstraint and extensive overconstraint. The lateral translation frequency increased from 4.6 to 5.3 Hz, indicating significant potential gain from HFOC. There is some discussion of this in report GMT6.pdf.

3. The effect of increasing c-ring width due to improved bending stiffness between c-ring brace nodes. It was concluded that the lateral translation mode frequency increased approximately 0.25 Hz per 250 mm of c-ring increased width. Although there is significant weight penalty and sacrifice of telescope compactness due to balance effects, this yielded a considerable gain. A brief discussion of this appears in GMT6.pdf. As a result of this study the c-ring width was increased from 1 to 1.25 meters.

4. The effect of pier and soil support compliance on modal performance. It is estimated these effects will lower the first fundamental frequencies by 0.2 to 0.25 Hz. The work is discussed in some detail in section 7.5 above and reports GMT7.pdf through GMT9.pdf.

5. A conventionally-stiffened azimuth structure which relied on steel to compensate for eccentricities between the OSS and pier support points was designed and optimized. Subsequently, the OSS support pedestal azimuth structure, in which the eccentricities are minimized and stiffened more directly by the pier was analyzed and determined to be superior. Although numerous structural refinements were made to the OSS between the two models, the first pedestal model was found to have a lateral translation frequency of 5.1 Hz as compared to 3.9 Hz for the optimized conventionally-stiffened azimuth system. The azimuth structure optimization is presented informally in GMT3.pdf.

It is noted that the last published data for GMT modal performance (Gunnels 2004) stated that the lowest telescope frequency was 5.1 Hz. This was for the complete rotating telescope structure but not including pier compliance effects. More detailed analysis has revealed that the earlier models were non-conservative in two respects. First, the stiffness used for the individual drive assemblies was found to be unrealistically high. Adopting values representative of the LBT gear drives reduced the drive stiffness by a factor of four. Second, the relatively coarse finite element mesh in the area of the hydrostatic pads was found to overestimate the local stiffness by a similar factor. The net effect of these two changes to the model was to lower the fundamental mode frequencies by about 0.5 Hz.

Also, since the SPIE report, numerous other refinements have been incorporated in the design. Some have slightly reduced the fundamental mode frequencies and others have slightly raised them with essentially a negligible net change. The current modal analysis results are summarized in Table 7-5.

Table 7-5. Model GMT158 Modal Analysis Results – Rotating Telescope Assembly (see section 7.5 for additional pier effects).

Mode No.	Natural Frequency (Hz)	Modeshape FM = fundamental mode PM = principal mode)
1	4.5	1st Lateral translation FM
2	5.3	1st Fore-aft translation FM
3	5.4	1st Azimuth rotation FM
4	7.46	2nd Fore-aft translation PM
5	7.49	2nd Lateral translation PM
6	8.0	Truss optic axis rotation
7	9.6	2nd Azimuth rotation PM
8	10.6	1st Vertical translation FM

7.6.2.2 Fundamental and Principal Modes of Vibration

The telescope structure is a distributed spring/mass system cantilevered from the top of the pier with its free end at the M2 assembly. It has multiple degrees of freedom in the sense that it consists of multiple masses and springs but also in the sense that it can vibrate in 3-dimensional space. Therefore, it has "lateral" modes, "fore-aft" modes, and "azimuth rotation" modes. Modal analysis of such a system reveals sets of *principal* modes of vibration in which the entire structure vibrates at one of the system's *natural frequencies*. In the *fundamental* modes (the lowest frequency, or first principal modes), all motion is in phase both in time and space. That is, all points in the structure move in the same direction and reach their peak amplitudes at the same time. In the second principal modes (next higher frequency) the free end of the structure is out of phase with the lower end of the structure. That is, there is an inflection point above which points move in one direction while points below move in the opposite direction, but they still reach their peak amplitudes at the same time. In the third principal modes (yet higher frequency), the free end and lower end are in phase but a central area is out of phase with them, etc.

Since there are three translational degrees of freedom for the system, there are three translational sets of these fundamental modes: lateral, fore-aft, and vertical translation. However, it is usually the case that lateral and fore-aft translation modes have relatively low frequencies and vertical translation (a more nearly axial phenomenon) a considerably higher frequency. Usually the vertical translation frequency is so high that the mode is not a concern. For the analysis summarized in Table 7-5, vertical translation barely appears as the highest frequency mode listed at 10.6 Hz. Figure 7-29, Figure 7-30, and Figure 7-31 below are the mode shapes for the fundamental modes for lateral translation, fore-aft translation, and azimuth rotation, respectively.

7.6.2.3 Dynamic Response Analysis (Wind Shake)

Subsequent to the basic design and optimization of the structure using modal analysis, a random vibration analysis has been performed. Although discussed in some detail in section 7.6.3 below, a few words are appropriate here.

The modal analysis was used to minimize the fundamental mode frequencies with essentially no value placed on raising the second and higher principal modes. One of the most important outcomes of the dynamic response analysis was learning that the line of sight (LOS) pointing errors due to wind excitation were much higher for the higher modes than for the fundamental modes. And in fact, those (large) errors were reduced dramatically by making changes to the structure that actually slightly reduced the fundamental mode frequencies. It is suggested that the second and higher principal modes may depend on different stiffness properties of the truss than do the fundamental modes. This seems apparent when one compares the modeshapes. For example, in the second fore-aft translation mode the M2 tilt is about 6 times larger than in the fundamental (first) fore-aft mode when scaled to the same peak deflection. Details of these and other issues are presented in section 7.6.3 below.

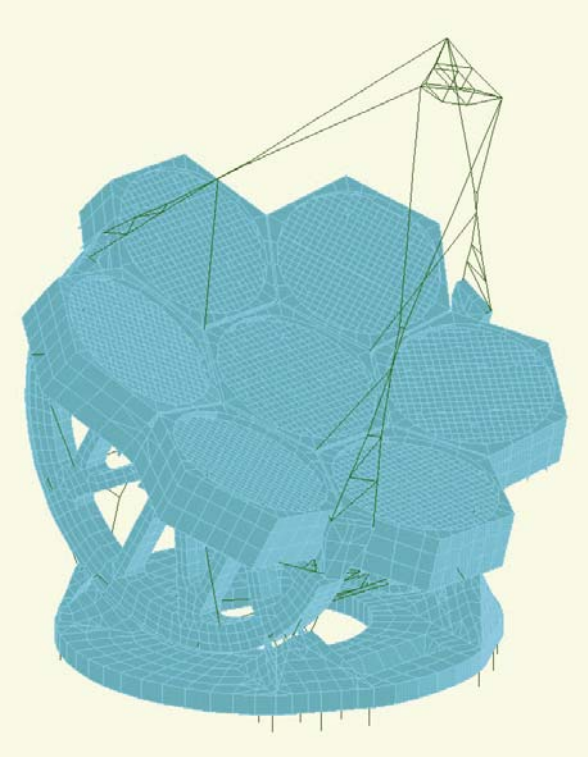

Figure 7-28. View of finite element model GMT159. See Figure 7-4 through Figure 7-6 for current upper truss and CCF brace geometries.

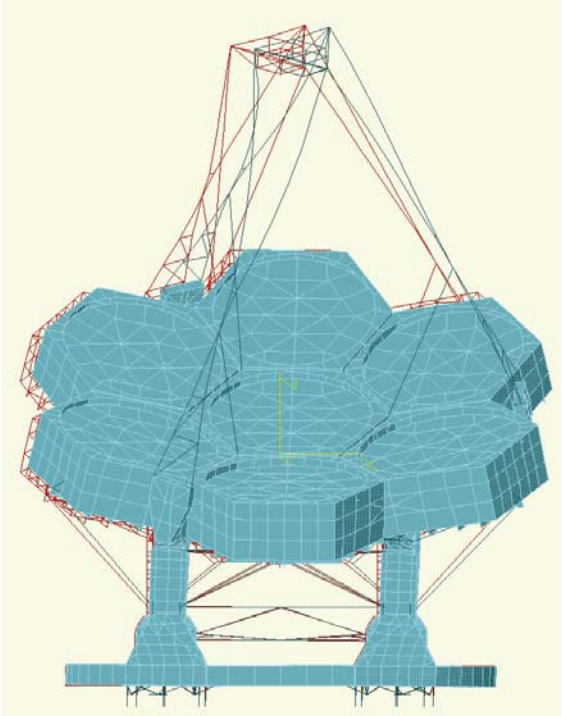

Figure 7-29. Mode 1, lateral translation.

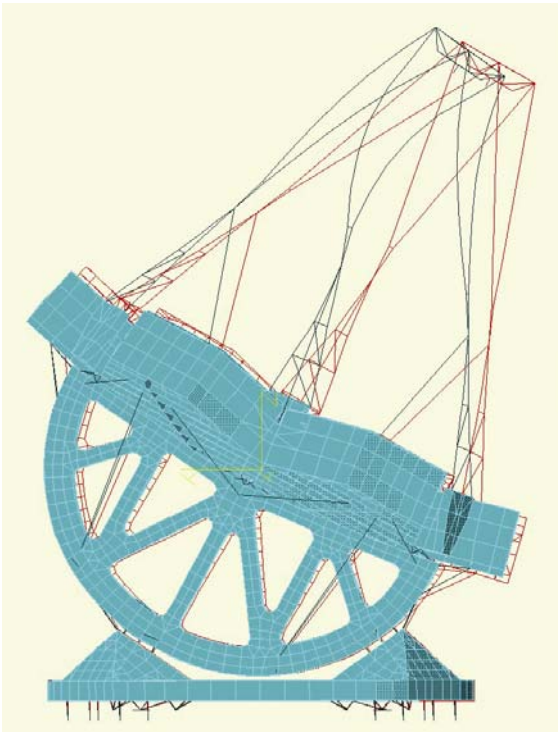

Figure 7-30. Mode 2, fore-aft translation.

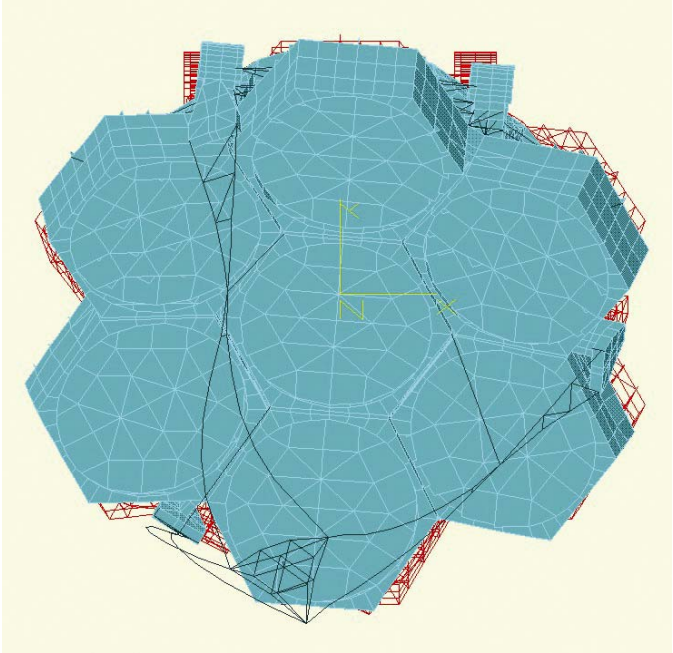

Figure 7-31. Mode 3, azimuth rotation.

7.6.3 Wind Dynamic Response

7.6.3.1 The Model

GMT commissioned a study by Simpson, Gumperz, and Heger to study the dynamic effects of wind on the GMT structure (GMT Document 1356), Appendix 7-2. The results are summarized below.

The purposes of the wind vibration analysis were:

- To study the dynamic response of the Giant Magellan Telescope (GMT) baseline structure to wind disturbance with the goal of determining order of magnitude motions of the optical components which include the primary mirrors, the secondary mirrors, and the Instrument Platform.

- To identify possible changes to the structure to improve the pointing accuracy of the baseline telescope.

The steps in the process were:

1. Confirm natural frequencies and mode shapes of the baseline configuration after converting the GMT ALGOR FE model developed for the modal analysis to MSC/NASTRAN,

2. Enter the optical sensitivity equations into the FE model that give image motions and focus changes in the subapertures due to displacements of the primary mirror segments, secondary mirror assembly, and Instrument Platform,
3. Calculate the dynamic wind load of the GMT structure and primary mirrors based on pressure and wind speed measurements at the Gemini South telescope prior to installation of the primary mirror,
4. Perform random response analysis to determine the response to dynamic wind loads,
5. Identify areas in the structure that significantly affect the pointing error and perform a sensitivity study on alternative configurations, and
6. Incorporate configuration changes in a final model and repeat the analysis.

To model wind on the primary mirror segments, time-sequence wind pressures from taps on the dummy mirror in the Gemini tests were applied to the surface of a GMT segment and the resulting power spectra of forces and moments on the segment were recorded. For the random response analysis, the forces and moments were applied to the segments supported on their hardpoints. It was assumed the forces between the segments were uncorrelated which is consistent with the lack of correlation on smaller spatial scales in the Gemini tests.

The secondary mirror assembly was assumed to behave as a rigid (non-segmented) body supported by the top frame of the telescope by a hexapod truss.

The results were calculated for 0.1 Hz to 25 Hz. Two values for the structural damping were investigated: 2% and 0.5%. The effect of locked versus free rotors on the drive motors was also investigated.

The Gemini data (Smith 2000)[1] used for this analysis was taken for two configurations: (1) enclosure vent gates open and wind screen open and (2) vent gates and wind screen closed. The telescope was set at zenith angle 30° and the external wind speed was approximately 13 m/s in both cases. At Las Campanas Observatory, this represents the 90^{th}-95^{th} percentile wind speed depending on the site.

Four different conditions were analyzed:

Condition 1: Vents and wind screen open, locked drive rotors, and 2% damping.

Condition 2: Vents and wind screen closed, locked drive rotors, and 2% damping.

Condition 3: Vents and wind screen open, locked drive rotors, and 0.5% damping.

Condition 4: Vents and wind screen open, free drive rotors, and 2.0% damping (discussed in Appendix 7-2).

7.6.3.2 Wind Study Results

A set of initial results were obtained for the original baseline GMT configuration. Figure 7-32 shows the PSD for pointing errors in the vertical (Y) direction. The individual curves are for the

[1]Gemini Data Viewer is available at: http://www.aura-nio.noao.edu/studies/wind_tests1/tests/index.html

7 subapertures and the blue line is the average weighted by area to take into account the hole in the center mirror. By inspection it is clear that most of the pointing error comes not from the lowest fundamental modes around 4.5 Hz but from modes in the 7-9 Hz range. This is even more apparent in the integrated PSD, Figure 7-33. The animated mode shapes show pronounced translation and rotation of the secondary mirror assembly relative to the primary mirror for these modes.

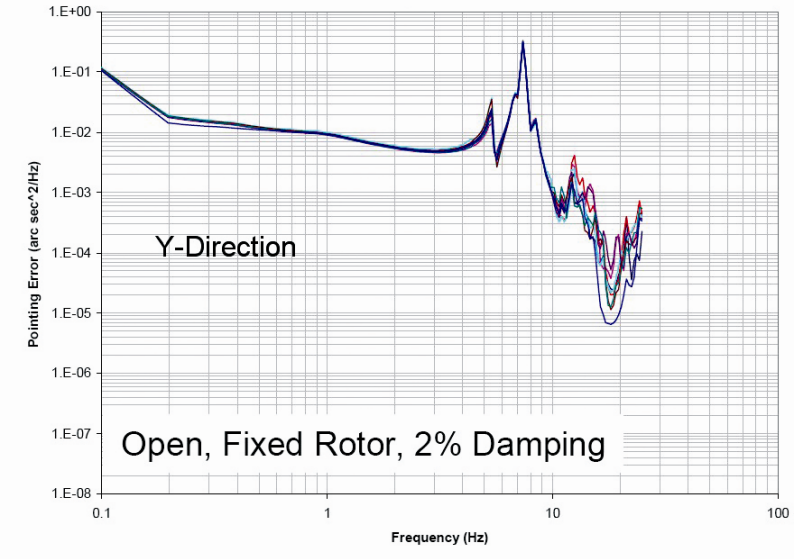

Figure 7-32. Baseline model. PSD of the Y-pointing errors.

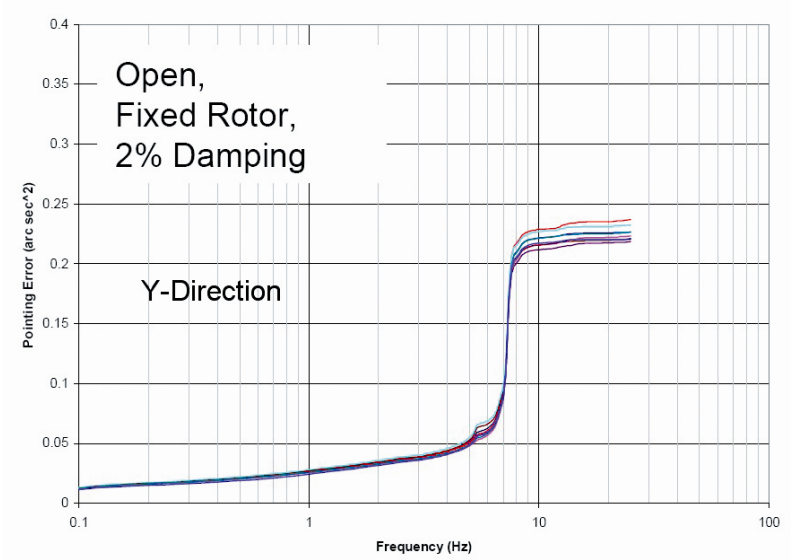

Figure 7-33. Baseline model. Integrated Y-pointing errors.

Based on the initial results the following changes were made to the GMT structure to reduce the pointing error:

- Bracing was added between the support pads at the base of the truss and the mirror cell to reduce rotation of the pad.

- Cross bracing was added between the upper legs of the truss to stiffen them in-plane.

- The wall thicknesses and moments of inertia of the upper truss legs were doubled.

The new braces are shown in the circles on Figure 7-34. The pointing errors were reduced roughly a factor of 2 by these changes. At the same time, the frequency of the two lowest fundamental modes of the mount structure were reduced ~0.05 Hz presumably due to the increased mass at the top end.

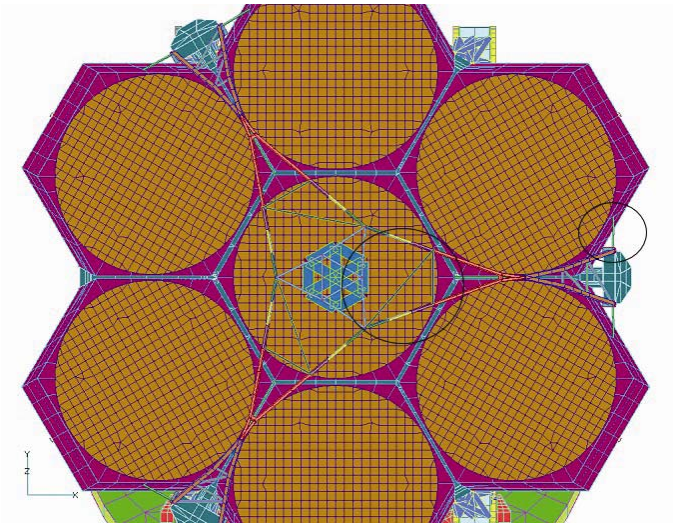

Figure 7-34. Revised bracing for the secondary truss.

Table 7-6 summaries the RMS pointing and focus errors. Appendix 7-2 shows mode shapes and PSD plots of the results.

Table 7-6. RMS Pointing and Focus Errors for Recommended Configuration.

	Analysis K Case 1 – Open Locked Rotor 2% Damping	**Analysis L Case 2 – Closed Locked Rotor 2% Damping**	**Analysis M Case 1 – Open Locked Rotor 0.5% Damping**
	RMS Pointing Error X Direction (arcsec)		
Minimum	0.106	0.036	0.209
Maximum	0.117	0.040	0.236
Weighted Mean	0.091	0.035	0.184
	RMS Pointing Error Y Direction (arcsec)		
Minimum	0.196	0.077	0.355
Maximum	0.211	0.083	0.394
Weighted Mean	0.195	0.078	0.364
	RMS Focus Error Z Direction (mm)		
Minimum	0.121	0.046	0.223
Maximum	0.230	0.074	0.431
Weighted Mean	0.143	0.052	0.271

7.6.3.3 Discussion

The analysis to this point has used the wind data results from the Gemini South because that study contains one of the most comprehensive sets of pressure and velocity measurements on an actual telescope structure. Time history records and power spectral density curves are available for a variety of cases. The dynamic wind loads on the GMT structure were calculated by adjusting and adapting the pressure and velocity measurements from Gemini South.

However, this approach has its limitations:

- The shape and scale of the Gemini enclosure is different from the GMT carousel-type enclosure. The arrangement of the shutters and vents for the two enclosures will be different and the secondary mirror of GMT will be recessed farther into the structure.

- The two telescope structures and secondary support structures do not share a lot of similarities and wind flow around the two will be different.

- All of the Gemini data used for this study were taken with the wind screen open. GMT will use the vertical shutter of the enclosure to shield the telescope from wind.

During the design development phase (DDP), computational fluid dynamics (CFD) of the GMT enclosure and telescope structure perhaps backed up by wind tunnel tests will be used to better determine the wind disturbance on the GMT structure. This will be applied to the structure in later rounds of dynamic response studies.

The top end of the telescope still contributes most to the pointing error due to bending in the truss structure and displacement of the secondary mirror support frame. Additional design effort will be put into this area to reduce the effect.

Damping also has a significant effect on the dynamic response of the telescope structure. This will be investigated more in the DDP and care will be taken in the design to ensure the telescope is adequately damped.

These initial results obtained for observing directly into a 13m/s wind, although not yet meeting the image error budget, are encouraging. Depending on the results of the flow modeling and servo analysis for the main drives, additional optimization of the structure and use of the wind screen will reduce the pointing errors and may be enough to achieve the error budget specifications without additional measures.

However, both of GMT's proposed secondary mirrors, the Adaptive Secondary Mirror (ASM) and the Fast-steering Secondary Mirror (FSM), have fast tip-tilt capability conjugated to the primary mirror segments to address the problem of wind shake. The small tilts required are within the range of throw for both mirrors.

7.7 Mechanisms

7.7.1 Main Axis Bearings

Typical of altitude-over-azimuth telescope mounts, GMT has six degrees of freedom to be defined for the OSS to the azimuth structure, and six degrees of freedom to be defined for the azimuth structure to ground. With the two axis rotations being accomplished with friction or gear drives this leaves ten degrees of freedom to be defined with bearings.

The issue of whether friction or gear drives are used is addressed briefly in Section 7.7.2 below. If friction drives are finally selected for the azimuth drive, a minimum of four approximately 750 mm diameter drive rollers could be used not only to drive the telescope but also to define the two horizontal translation degrees of freedom for the azimuth structure to ground. Preliminary calculations indicate that the azimuth drive/positioning rollers would have adequately high stiffness, would be robust (have low Hertzian stresses at the roller contacts) and would have acceptably low friction. In that case three degrees of freedom remain to the defined with the azimuth bearings.

Table 7-7. GMT Axis Definition, Bearings and Drives.

Axis Definition	Bearing Set	Dof's	Master Pads	Slave Pads (HFOC)	Total Pads
OSS-to-Azimuth	OSS radial pads (4 sets of 6)	4 Ytxl Ztxl Yrotn Zrotn	4	20	24
OSS-to-Azimuth	OSS lateral pads (4 sets of 2)	1 Xtxl	1	7	8
OSS-to-Azimuth	(Altitude Drive)	1 (Xrotn)	-	-	(8 drives)
Azimuth-to-ground	Azimuth vertical pads (4 sets of 6)	3 Ztxl Xrotn Yrotn	12	12	24
Azimuth-to-ground	(Shared azimuth drive/position rollers - position rollers)	2 Xtxl Ytxl	2 (rollers)	2 (rollers)	(4) (position rollers)
Azimuth-to-ground	(Shared azimuth drive/position rollers - drive rollers)	1 (Zrotn)	-	-	(4 drives)

Due to their high local load capacity, high stiffness and very low friction, hydrostatic bearings will be used for all other axis definitions. Table 7-7 summarizes the GMT baseline design drives and bearings complement. Refer to the Design Requirements Document in Appendix 7-1 for coordinate system definition.

The total number of bearings used to define and support GMT is greater than the ten degrees of freedom that require definition (ref. paragraph 1 above). Since all of these bearings have measurable stiffness, the system is "over constrained" by the conventional definition. Two methods are used to avoid problems associated with over–constraint, primarily load variations in the bearings that could lead to film failure causing high friction and bending of the OSS causing alignment problems. The first involves designing the over-constrained bearings with "high frequency over constraint" (HFOC) that allows them to provide a stiff load-path at moderate- and high-frequencies but enables them to adjust their length at low frequencies and re-distribute the load to the other bearings.

In HFOC two types of bearings are used to define a subject degree of freedom: master and slave. The master bearings shown in Figure 7-35 are articulated to eliminate over-constraining moments at the interface but are rigid in the load-carrying axial direction. The slave bearings incorporate an internal hydraulic piston in the pad design that allows them to carry their portion of the load but also adjust to height variations of the track. The pistons also provide the required articulation in angle. A flow restrictor in the oil supply line to the preload piston causes it to become stiff at high frequencies above around 3 Hz. This constitutes an over-constraint at those relatively high frequencies that greatly contributes to the overall stiffness and modal performance of the structure, yet allows the pads to compensate for manufacturing irregularities and thermal distortions that develop slowly (<1 Hz). For frequencies $\geq$ 3 Hz the slave bearings are as stiff as the master bearings.

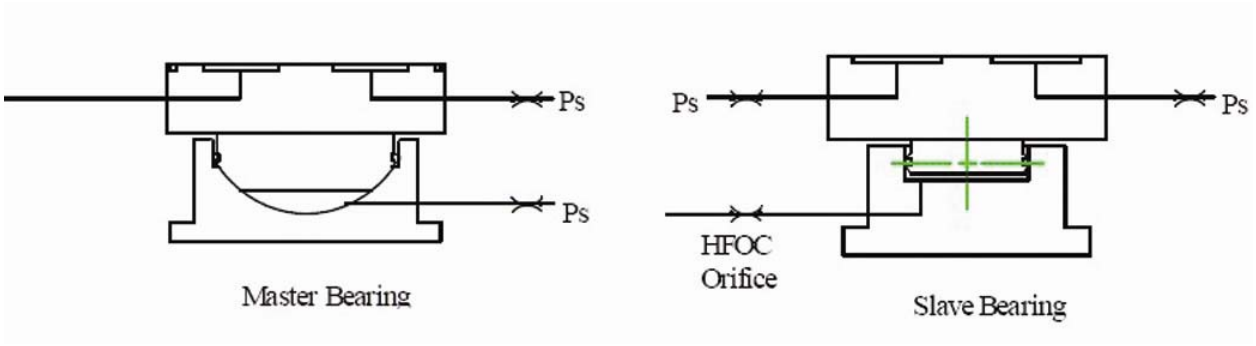

Figure 7-35. Master & slave hydrostatic bearings.

The second method for dealing with the problem relies on global compliance in the structure to prevent high stresses developing across the structure as a result of the over constraint. Multiple local areas of the structure are fully constrained for a subject degree of freedom yet the structure is globally compliant in a way that allows each local area to accommodate irregularities without large force variations in the pads.

From Table 7-7, five translation and rotation degrees-of-freedom are defined on the OSS by five master bearings. The sixth DOF, altitude rotation, is provided by the drives. The additional 27 OSS bearings use HFOC. The arrangement provides a kinematic support that is not over-constrained.

On Azimuth, 12 master bearings plus 12 HFOC bearings are used to define only 3 degrees of freedom. The over-constraint can be tolerated because the very large (21 meter diameter) and relatively thin (1 meter) azimuth disk will bend out-of-plane to accommodate small irregularities of the azimuth runner bearing causing only small force variations in the hydrostatic pads as the telescope rotates in azimuth. The relative motions of the sets of bearing at the four corners of the azimuth structure will cause small, slowly varying pointing errors that will be corrected with the pointing model and guiding in the telescope control system. The other two azimuth degrees of freedom, lateral x and y translations, use HFOC on the preload rollers. And finally, rotation about the azimuth axis is defined by two of the rollers being drive rollers.

The hydrostatic bearings are critical for the modal performance of the telescope and a substantial amount of effort has gone into optimizing the bearing design. Trade studies of various bearing pad geometries were conducted to investigate the differences in film thickness and flow rates as functions of pocket pressure, temperature, and pad velocity. Attention was focused on two aspect ratios looking for variations in film thickness due to structural deflection of the runner bearing: (a) “long” pads 762 mm long by 267 mm wide and (b) “short” pads 585 mm by 305 mm. The short pads were found to have +/- 6 microns variation, the long pads +/- 8 microns (Gunnels 2004). The short pads were selected for the baseline design on the basis of manufacturing considerations of the bearings and runner surfaces and lower deflection. The bearing and hydraulic system designs are described in GMT Document 1131 (Chivens, 2005).

Trade-off studies for oil flow regulation to the pads lead to the selection of capillary flow restrictors over orifices or flow control valves. The capillaries maintain constant film thickness and hence bearing stiffness over the full operating temperature range.

Properties of the GMT hydrostatic bearing system are listed in Table 7-8.

Table 7-8. Hydrostatic bearing parameters.

Design load per bearing	38 metric tons	
Operating temperature range, T	-9 °C to +27 °C	
Pad size:		
Overall	305 mm x 585 mm	
Active area	280 mm x 560 mm	Recess pocket plus lands
Recess pockets per pad	4	
Radius of curvature, R		
OSS radial	10.4 meters	Cylindrical surface.
All others	plano	
Oil type:	Mobil DTE 13M	Same as Magellan.
Flow control method:	Capillary	
Oil film thickness, τ:		Design values.
Nominal, τ_{nom}	50 microns	
Maximum, τ_{max}	75 microns	
Master bearing stiffness:		
Nominal oil film stiffness	14.7 kN/ μm	τ = 50 μm, T = 27°C
Stiffness including spherical seat	7.5 kN/ μm	τ = 50 μm, T = 27°C
Minimum film stiffness @ τ_{max}	9.8 kN/ μm	τ = 75 μm, T = 27°C
Min. stiffness with seat @ τ_{max}	6.0 kN/ μm	τ = 75 μm, T = 27°C
Oil pressures:		
Pad recess	3.2 x 10^6 Pa	
Spherical bearing	5.6 x 10^6 Pa	
System pressure	11 x 10^6 Pa	
Flow rate:		
Nominal per pad @ T_{max}	1.67 l/min	τ = 50 μm, T = 27°C
Total flow including seat	1.82 l/min	τ = 50 μm, T = 27°C
Maximum flow @ T_{max}	5.77 l/min	τ = 75 μm, T = 27°C

7.7.2 Main Axis Drives

The telescope drives must smoothly and stiffly control the OSS and azimuth structure as the telescope precisely tracks astronomical objects across the sky. They must also overcome inertial and wind loads and operate reliably (although with lower precision) at slew rates between observations.

GMT uses "direct gear drives" on the elevation axis for the baseline design. Each of the eight assemblies would be similar to those used by the LBT project, shown in Figure 7-36. They consist of a frameless Kollmorgen/Inland motor in a custom housing directly driving a pinion. The drive reduction ratio for the axis is the ratio of the pitch radius of the bull gear to the pitch radius of the pinion. Although the mechanical design of the drive and bull gear mounts has not yet been undertaken, the structural stiffness of these drives has been included in the modal and dynamic response analyses.

The GMT azimuth axis will use four friction drives. In this case the pinion is replaced with a friction roller which drives against the inside diameter of the azimuth track. The four friction roller drive units are also used to define the azimuth axis ("X" and "Y" position for the telescope). An internal reduction stage may be required on the azimuth drives to accommodate the large diameter (750 mm) friction roller.

Figure 7-36. Photo of LBT drive motor housing.

7.7.3 Instrument Platform Assembly

For reasons detailed in 7.2 (Overview), the GMT project elected to not implement a classical Nasmyth focus. Therefore, all instruments are mounted on the Instrument Platform Assembly which is supported by the C-rings below the primary mirror cells. As shown in Figure 7-37 to Figure 7-39 below, the assembly includes a large stationary structure - the Instrument Platform (IP) - and the Instrument Rotator which is supported by the IP. Various instrument mounting configurations are available:

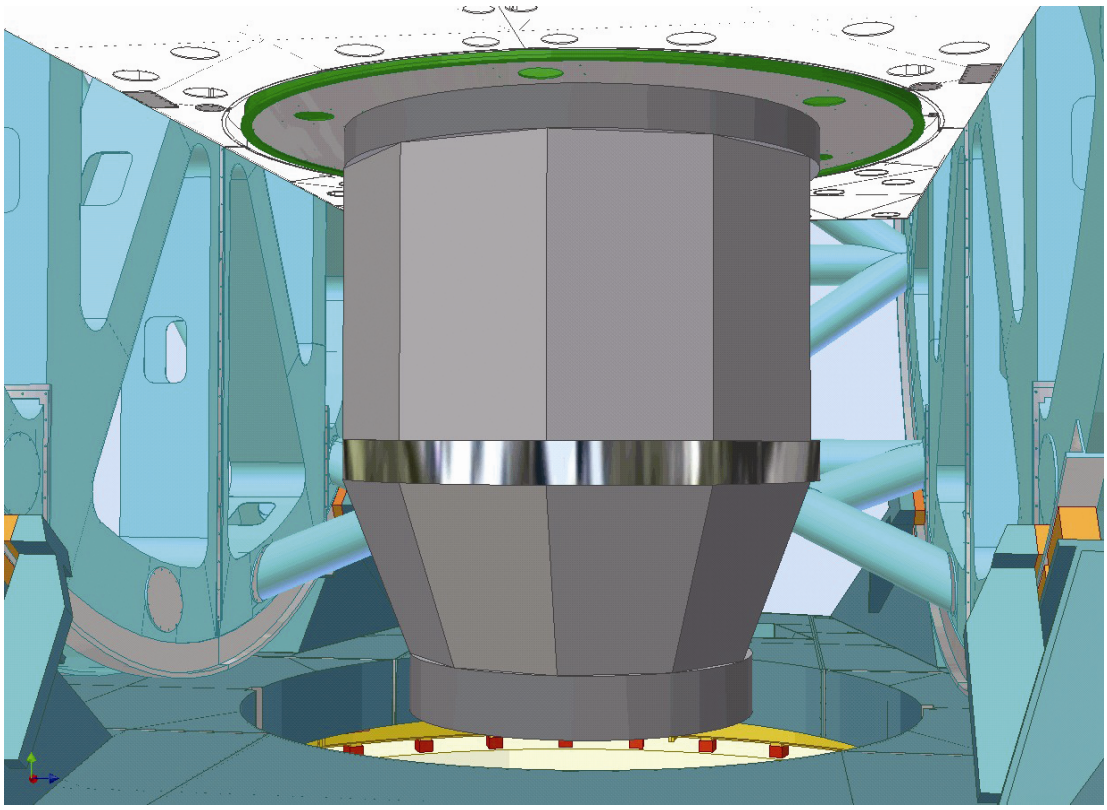

Figure 7-37. Underside view of IP and Instrument Rotator with notional Gregorian instrument.

1. **Gregorian** – On the underside of the Instrument Rotator with direct light feed from above. Very large instruments can be mounted here, up to 6.4 meters in diameter by 7.6 meters long and weighing up to 23 metric tons. A notional instrument is shown in Figure 7-37. Changing such instruments is done by the Central Lift (section 14.8.1) during the day. Alternatively, multiple smaller instruments can be mounted in an instrument module with changes between these instruments made during the night. Flexure compensation due to these large instruments rotating in the gravity field will be done by astatic levered rollers or active compensation within the instruments, or both.

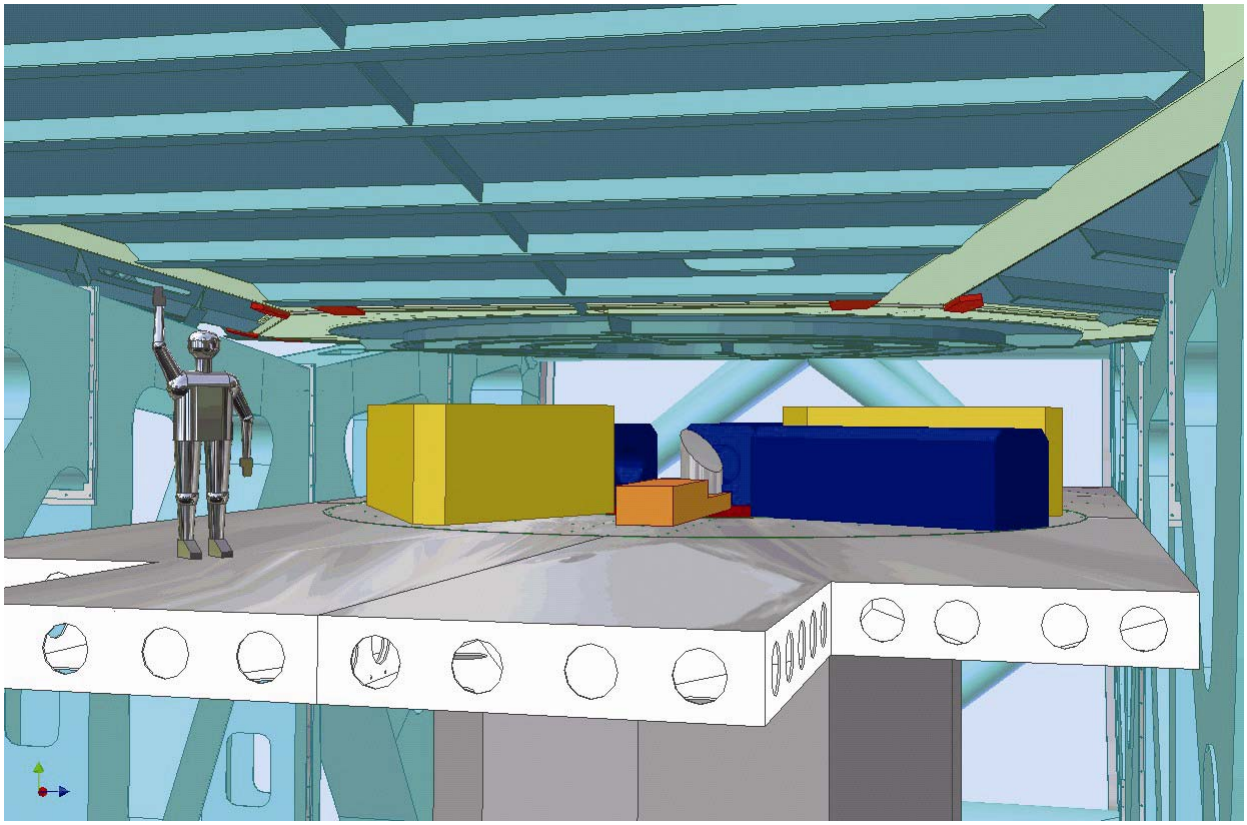

Figure 7-38. Topside view of Instrument Platform (IP) and Instrument Rotator with notional folded-rotating instruments.

2. **Folded-rotating** – On the top side of the Instrument Rotator with the beam reflected to one of six positions. Smaller instruments are mounted here – notional instruments are shown in Figure 7-38. The vertical space available for these instruments is limited by the underside of the center mirror cell and is currently 1.9 meters. The total payload for folded instruments is 11.3 metric tons. Although this defines an average instrument weight of 1,900 kg, an individual instrument could be much heavier. Instrument changes are made via the IP extension at the back of the telescope using a lift from the observing floor.

3. **Folded-stationary** – On the top side of the IP. Since this structure is stationary, rotating and guiding is done by a local opto-mechanical assembly within the instrument. Although an instrument mounted in this way would fall within the 11.3 metric ton upper instrument payload, it could employ a rather long reimaged light path. It is tentatively planned that the multi-conjugate adaptive optics instrument (MCAO) will be mounted in this way. Instrument changes are done as with folded-rotating instruments.

4. **Gravity invariant** – One additional mounting location is under consideration which is an extension of the folded-stationary concept. In this case the optical beam would be relayed parallel to the elevation axis through an opening in one of the c-rings to an instrument mounted on a bearing outside of the c-ring. The instrument would rotate to

maintain a gravity invariant orientation as the telescope rotates in elevation.

Preliminary design work has been done on the rotating platform bearing. Because of its large size (8.9 meter diameter) and considering related issues of friction, cost, and shipping, a custom adjustable roller support is tentatively planned. Using three sets of six 100 mm rollers, the bearing can be kinematic and adjustable to control preload. Both of these features will contribute to the bearing having low friction which will benefit the rotation drive control. The Instrument Rotator is removed by the Central Lift prior to lowering of the center mirror cell for recoating (Section 14.8.1).

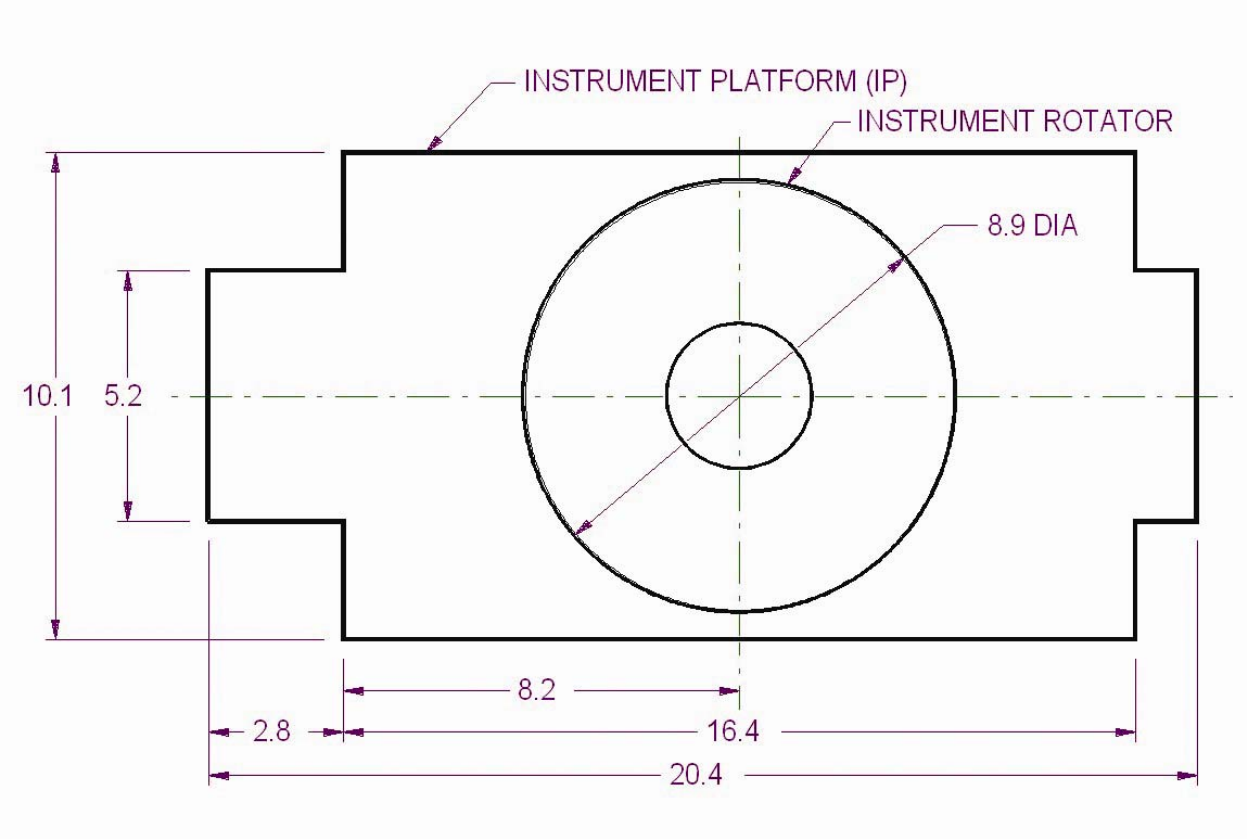

Figure 7-39. Instrument Platform (IP) and Instrument Rotator dimensions (meters).

7.7.4 Mirror Covers

Mirror covers are desirable on optical telescopes for a number of reasons. For example, they can:

- Protect the glass from hazards falling from above.
- Minimize dust that would otherwise settle on the glass surfaces during the day.

- Minimize thermal loading (stresses on the mirror) during the day.

- Enable access to the top cell area, such as for connecting and rigging lifting cables.

Implementing mirror covers for even modestly-large telescopes has historically been very challenging - in fact, some telescopes do not even have covers. One of the advantages of an unfilled-aperture telescope is that it is possible to support sub-aperture covers of reasonable size. The GMT project feels that mirror covers are sufficiently important that we have developed two concepts, which are described below.

7.7.4.1 Rigid-panel mirror cover

This design is feasible partly because of the open access to the mirror segments afforded by the GMT secondary truss (the covers and access are apparent in Figure 14-19). The system, shown in Figure 7-40, consists of rigid lightweight panels that are semi-automatically installed and removed on the telescope each day.

The covers are aluminum honeycomb sandwich construction with approximately 1.25 mm thick aluminum skins separated by 150 mm thick aluminum honeycomb structural core material. They are edged with a rolled lightweight aluminum channel bonded to the skins. Similar panels were used on the Magellan telescopes but in a bifold arrangement (essentially four panels covering the 6.5 meter diameter primary). The central 2 meter region is reinforced structurally and includes six robust projections to allow remote latching to the underside of the lifting arm hub.

The 9.2-meter (maximum dimension) semi-hexagonal covers seal to the top surface of the non-structural cell top plate just outside the 8.6-meter diameter hole in that surface. The covers are coarsely registered and latched in place with remotely operated clamps or retention devices. Each cover assembly weighs approximately 600 kg.

The 6-step process to remove one mirror cover can be semi-automatic. It is controlled by an operator on a small platform attached to the enclosure, who is aided by two observers (one on the telescope, the other at the storage platform). It is estimated that the cycle time could be about 5 minutes per outer cover, or 40 minutes for all seven covers. The rotation of the telescope can be done while the lift assembly is transiting radially and thus does not add to the cycle time.

The seventh (center) segment cover is not yet defined. It is noted that, once the outer six covers are in place, access to the central mirror is improved. For example, a lightweight fabric cover could be fairly easily deployed by two persons using a long spool, while walking on the outer covers. A more robust center cover may be possible by using the outer covers as a work surface during deployment. The rigid-panel covers are sufficiently lightweight that it may even be feasible to reach the center mirror cell by telescoping the jib boom.

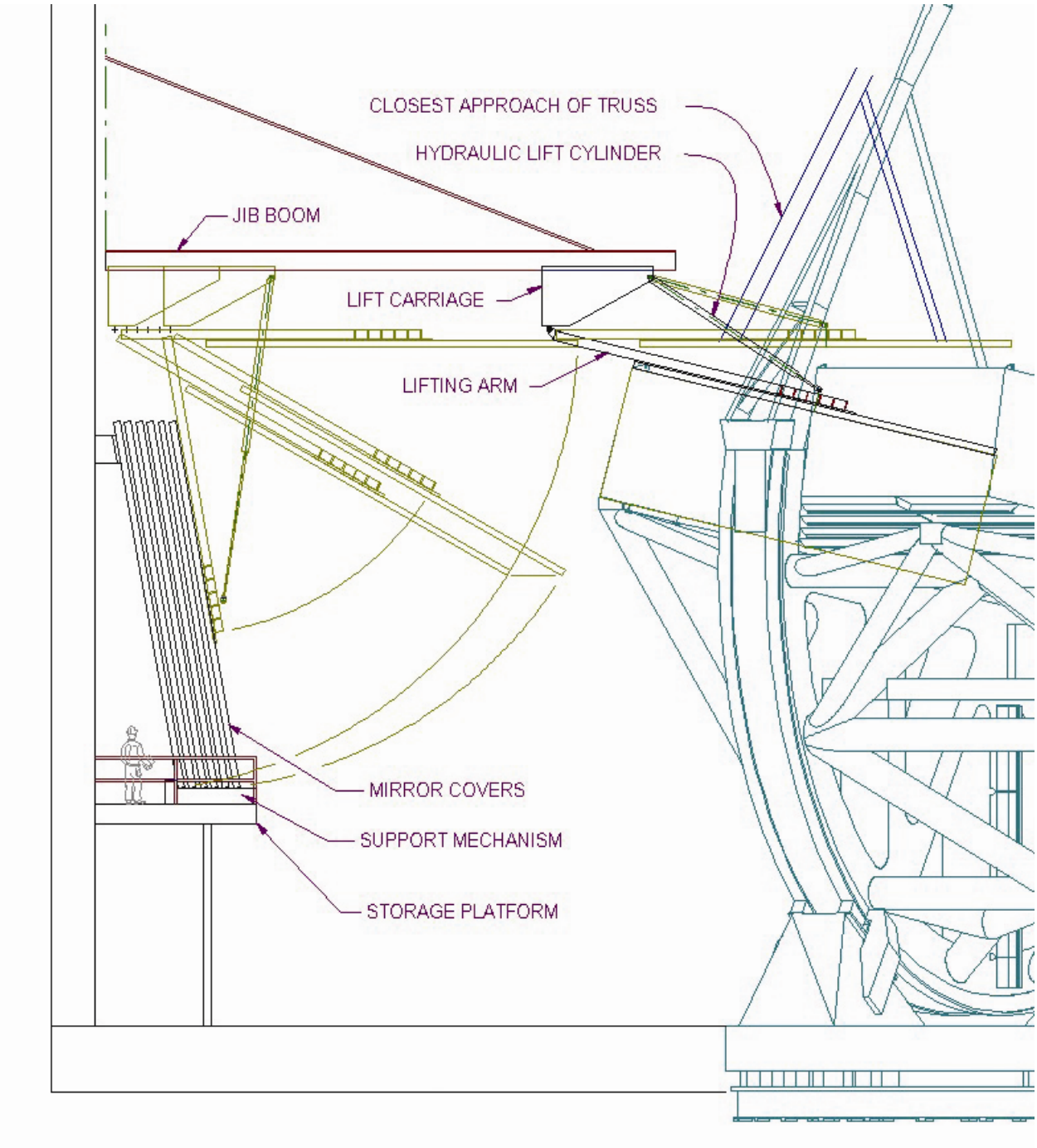

Figure 7-40. Side view of rigid-panel mirror cover system.

7.7.4.2 Hemispherical fabric mirror cover

A mirror cover that could remain on the telescope is shown in Figure 7-41. Each of seven 8.7-meter diameter covers would deploy over an individual segment. The hoop-and-fabric

construction would use a tough, lightweight material such as sail cloth. The moving weight of each assembly is estimated as 325 kg. As shown the system uses nine moving hoops, five of which are on a slightly smaller radius than the other four. With a tapered arcuate standing plate along the outer edge of the outer cells (at mid-radius between the hoops), the sections of fabric fold in a controllable way as the cover is opened. The deployment is driven by two rotary drives, one at each end of the cover. Opening or closing could be done quickly (approximately one minute each operation) using 1 h.p. motors. The cover assemblies would be removed for mirror coating. A more detailed description is included in GMT document no. 1097.

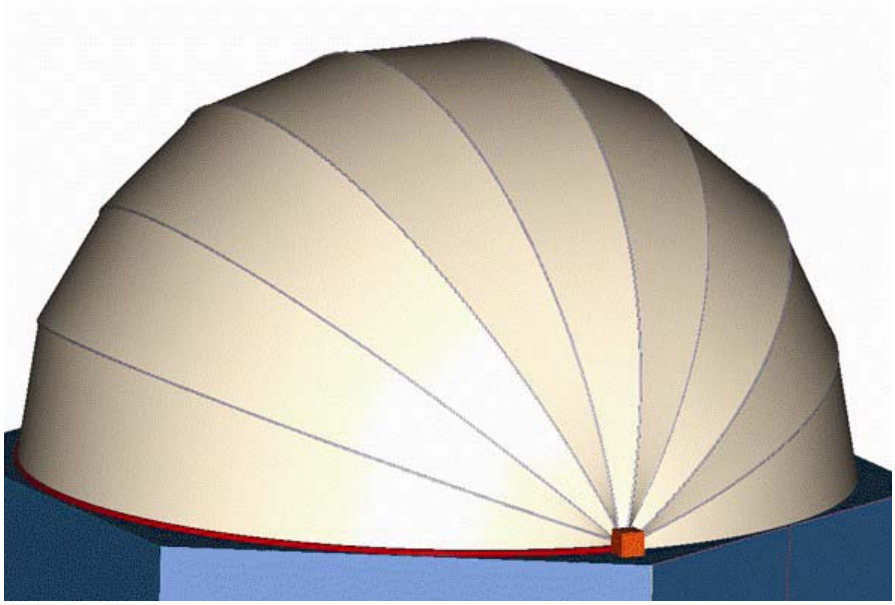

Figure 7-41. Hemispherical hoop-and-fabric segment cover.

7.7.5 Counterweights

The OSS must remain well balanced about the elevation axis at all elevation angles and with significantly varying payloads. By far the largest variable payload is the series of instruments that mount to the Instrument Platform and Instrument Rotator. The total instrument complement weighs 34 metric tons with its center of gravity. about 5 meters below the elevation axis. This moment is approximately four times the sum of all other variable moments for the OSS. Considering the large magnitude of this moment and the fact that it is desirable to keep the Instrument Rotator approximately balanced locally, we plan to exchange fixed counterweights with the large Gregorian instrument payload on the underside of the Instrument Rotator. (That is, if there should be no large Gregorian instrument mounted for a time, a fixed counterweight will be installed there.) This is easily done using the telescope central lift (ref 14.8.1).

The other significant variable moments for the GMT OSS are summarized in Table 7-9:

Table 7-9. OSS Variable Payloads and Moments.

OSS Variable Payloads and Moments				
Item	**Mass, kg.**	**Z, Y moment arms meters**	**Moment M_z, kg-m**	**Moment M_y, kg-m**
Mirror covers, rigid panel (7)	600 x 7	3.46 (Z)	1.5×10^4	n/a
Gregorian instrument axial travel	14,000	1.25 (Z)	1.8×10^4	n/a
M2 baffle	90	22.3 (Z)	2×10^3	n/a
Residual instrument	(5% of total)	5 (Z)	9×10^3	n/a
Corrector lenses in/out of beam	1,800	2.2 (Y)	n/a	3.90×10^3
Total moments	-	-	**4.40×10^4**	**3.90×10^3**

The GMT project initially planned to use a system of powered mechanical counterweights for smaller payloads and fixed counterweights for the larger moments. However, space for mounting and accessing these mechanical assemblies is becoming encumbered by other systems such as the housing for the AO lasers (cf. Chapter 9), the central lift travel envelope, stairs and platforms and possibly future mounting of instruments on the outside of the c-ring. Therefore, we are considering implementing a fluid counterweight system similar in principle to that used by the LBT project.

Shown in Figure 7-42, the system uses three stainless steel tanks mounted in available space between the c-ring spokes. With the volume of the lower tank equal to 150% of that of each of the upper tanks, and considering the relative position of the three tanks, fluid can be pumped between the three tanks in a manner that compensates for both the large M_z and the much smaller M_y moments defined above. A small additional margin is required of the system so that the small M_y moment can be compensated simultaneously with a large M_z moment (that is, one cannot have all of the fluid in the lower tank and still compensate a small M_y moment).

As shown, the lower tank usable volume is 7,600 liters, or 7,285 kg of water if the tank thickness were equal to the 1.27 meter thickness of the c-rings. This would define an M_z moment of 3.9 x 10^4 kg-m simultaneous with the 3.9 x 10^3 kg-m capacity M_y moment required above. The additional moment required could be achieved by making the tanks thicker than the c-rings (say 1.5 meters), or making the lower tank a little larger. Alternatively, a much larger system and margin could be achieved by duplicating the system described in the other c-ring. If the fluid counterweight system is implemented in only one c-ring, the unsymmetrical loading would be only about 1.3% of normal gravity loading under the telescope weight. Some features that the system will require are:

- Numerous full-height baffles in the tanks, fabricated from perforated metal to minimize sloshing.

- Each tank will be mounted on three load cells (other degrees of freedom flexure-mounted) so that the balance can be accurately calculated.

- Overflow protection is required should the system try to overfill either of the two smaller tanks.

- It may be necessary for the system to calculate not only the load in each tank, but also its local c.g. location, and respond by moving fluid even during an observation. This is due to the small c.g. motions that result from the fluid moving in the tanks as the gravity vector varies during OSS rotation. The fluid is moved using a centrifugal pump and a series of directional control valves.

- An approximately 40% glycol solution would be used to prevent freezing at low temperatures.

We believe the proposed system has the advantages of having very large moment capacity, it minimizes the use of operations resources, it solves the space and access problem, and may be lower in cost.

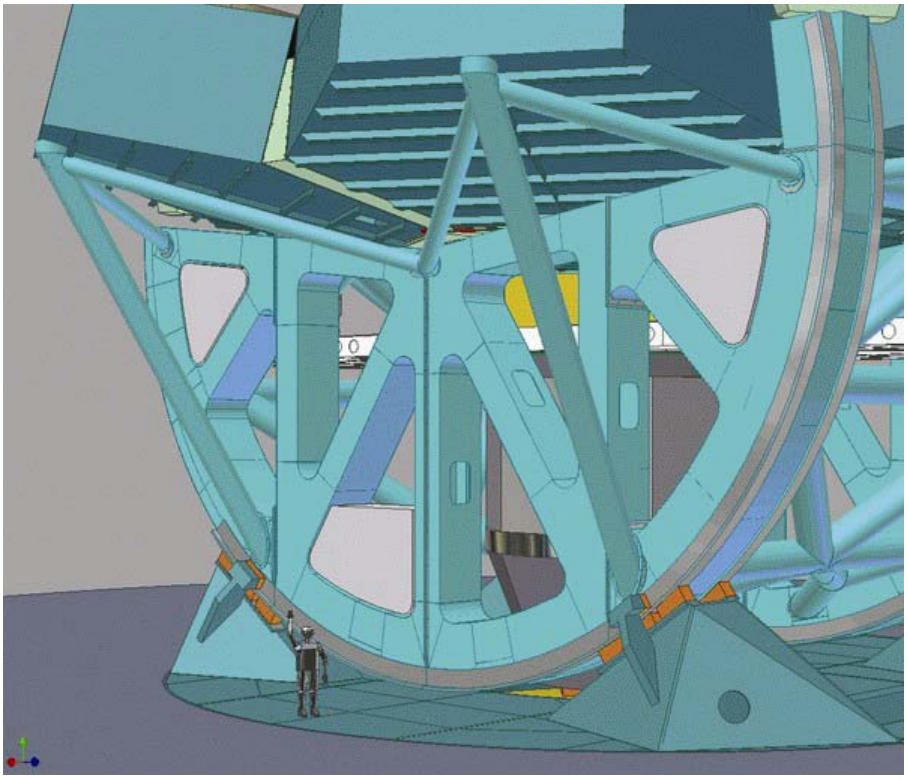

Figure 7-42. View of fluid counterweight tanks.

7.8 **Manufacturing Issues**

Most manufacturing challenges associated with building large telescope structures are a result of the high precision that is required of both the individual parts and the final assembly. In addition, increased size and weight of the parts can make both manufacturing and shipping more difficult.

Dimensionally GMT is about 2.5 to 4 times larger than Magellan (2.5 times in height, 4 times in diameter). The rotating weight of GMT is about 7 times heavier (1,000 metric tons vs. 135 metric tons). However, for both telescopes the maximum part size has been determined essentially by the diameter of the primary mirror. That is, with Magellan's primary 6.5 meters in diameter (and its shipping structure a little larger) the large structural parts were made about the same size to minimize the cost and weight of added manufacturing joints. And with GMT's primary segments 8.4 meters in diameter, the GMT large structural parts have similarly been made about 9 meters in size. For most of these large structural parts, both vendors who have provided cost estimates for GMT have accepted that they could fabricate, machine and ship the parts. One vendor suggested that a part could be separated into two slightly smaller units to facilitate handling and machining.

One manufacturing issue that is much more impacted by GMT's size is the shop assembly and test. Ideally the complete telescope would be assembled and tested in an enclosed facility

protected from the elements. We consider that, at a minimum, the structure from the azimuth track up through the primary mirror cells will be assembled and rotated on its hydrostatic bearings in both azimuth and elevation. The main axis drives will be installed and checked for fit. Without the secondary truss and M2 assembly the system could be functionally tested with the OSS balanced by reducing or eliminating the instrument and counterweight payloads. Doing this would reduce the height of the building required to clear the structure from 39 m to around 27 meters at GMT's minimum elevation angle.

There are a few detailed manufacturing challenges in GMT that were not present in the Magellan telescopes. The three most significant of these are described below.

7.8.1 C-ring machining and assembly

Hydrostatic pad runner bearing surfaces are critical in telescopes because they must be precise over the scale of the bearing pad size in order to reliably flow oil through the thin bearing gap (typically about 65 microns). In particular, the step between sections where the hydrostatic pads run across a manufacturing joint must be limited to perhaps 5 or 10 microns. The c-ring machining and assembly is somewhat more challenging than were analogous parts on Magellan. The altitude disks of Magellan had equivalent curved and flat precision machined surfaces that were runner bearing surfaces for the elevation hydrostatic pads. However, there were no manufacturing joints in these Magellan parts as there are in GMT. The c-ring is shown in the area of a manufacturing joint in Figure 7-43. While there were manufacturing joints on the Magellan ring beam (also a runner bearing surface), those were flat and could be blanchard ground as individual parts, then precisely adjusted and hand scraped to all but eliminate any steps.

Therefore, the machining and assembly of the c-rings is expected to be one of the more challenging manufacturing tasks. Machining of the c-rings might be done with one of three methods:

1. Pre-machine the interface joints, bolt the sections together, mount the assembly horizontally on a large vertical boring mill or similar machine, and machine the runner bearings with a single-point cutting tool. The surfaces could subsequently be ground with a portable grinding head (although this may not be necessary). If this method were used the c-ring design might be altered so that both c-rings could be mounted back-to-back and machined simultaneously.

2. Pre-machine the interface joints, bolt the sections together, mount the assembly horizontally on a large rotary table, and machine the runner bearings with a portable milling head. Grinding could also subsequently be done here, and doing the two c-rings simultaneously might also be an option.

3. Machine the individual sections separately on a CNC milling machine, such as a CNC gantry mill. This method would leave the largest differential dimensions between parts, requiring more challenging assembly adjustment.

The alternative options for machining and assembling the c-rings will be studied during the Design Development Phase.

7.8.2 Outer cell interchangeability

The seven outer cells (six active plus one spare) must be interchangeable with moderately high precision in order to minimize the mirror support system travel required to align the segments. $\pm$2 mm of actuator travel has been allocated to account for the cell installation variations. Since five degrees of freedom of each outer cell are defined at the CCF hub (see section 7.4.5.2) most of the precision can be achieved by accurate machining of the hub/cell interface areas. The precision of the sixth degree of freedom (the vertical support near the outer edge of the cells) will be achieved by adjustment of both the c-ring support points (at the quadrupods and tripods) and corresponding cell interface fittings at site assembly. This can be done in a two-step process:

1. Using one off-axis cell as a master, install and adjust its position in each of the six outer-ring positions using the c-ring support point adjustments and laser metrology to gage its position. This ensures that the geometry of the six c-ring supports is sufficiently accurate to accommodate manufacturing variations in the other cells and interchangeability.

2. Install the other six cells and adjust their interface fittings so that each is positioned with sufficient accuracy, again using laser metrology. This assures that the interface geometry of each individual cell is sufficiently accurate.

The combination of the two above procedures will assure that the cells interchange with sufficient accuracy to satisfy the actuator travel allocation.

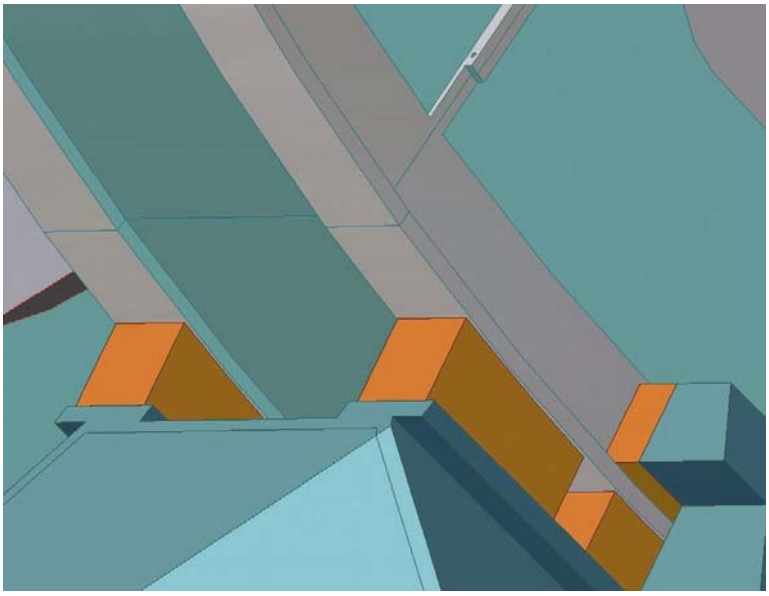

Figure 7-43. View of C-ring manufacturing joint.

7.9 Technical Challenges & Risks

A number of technical challenges and risks have been identified for the design, fabrication, shipping and assembly of GMT. These include:

1. **Wind shake**. GMT with lowest vibrational modes in the 4-5 Hz range is remarkably rigid for a structure of its size. Nevertheless, the preliminary dynamic response analysis indicates that for high-wind conditions uncompensated wind shake may exceed the error budget allowances. The measures being taken to address the problem are:

    a. The structure has been optimized for compactness and rigidity. Special attention will be paid in the design of joints, connections to the pier, pier design, and details of the bearings and drives to ensure that the final performance is not compromised. Further optimization of the top end of the telescope is expected to produce improvements in the modes most damaging to image jitter.

    b. A reduced cross section minimizes the wind forces on the upper structure and the amplitude of the disturbances. Further optimization of the shape factors of the truss members will be studied in the next phase. The secondary mirror assemblies will be designed for minimal cross section.

    c. The dynamic analysis shows the amount of structural damping has a large effect on the oscillation amplitude caused by wind disturbance. The preliminary analysis assumed an overall damping coefficient for all modes of 2% in one case and 0.5% in the other. Both passive and active damping will be studied in the next phase in order to suppress vibrations.

    d. Many factors in the design of the enclosure affect the amplitude and frequency spectrum of the turbulent wind flow acting on the telescope. The wind environment within the enclosure will be modeled and the results will guide the enclosure design to reduce wind disturbance.

    e. Fast tip-tilt steering motion is provided in the secondary mirrors. A fast read-out camera in the focal plane will sense image motion in the 7 subapertures and provide error signals to the image stacker system for guiding out wind shake.

2. **C-ring manufacture**. The c-rings are large assemblies with continuous precision surfaces many meters long extending over multiple segments. The manufacture and assembly of these parts present special challenges as discussed in Section 7.8.

3. **Structure alignment**. The alignment of the GMT structure during assembly at the fabricator's plant and on-site will require special metrology and fixturing that will have to be defined and included in the preliminary design well prior to start of manufacturing. The advent of laser ranging metrology provides new techniques not possible a few years ago. Alignment procedures will be documented and placed under configuration control by the time of preliminary design review.

4. **Slave/master bearing ratio**. The hydrostatic bearing system on GMT consists of master and slave bearings (Section 7.7.1). Once the pads have set down on their track, the master bearings retain their axial and lateral stiffness when oil pressure is removed. The same is not true for the slave bearings. They may be designed with some lateral stiffness but they provide no axial support once the piston pressure has bled down. The ratio of slave to master bearings varies depending on location on the structure but is as high as 8:1 for some bearing groups. The master bearings will be designed to carry the full load of the telescope even when the oil pressure is off and the slave bearings are inactive. This applies to both static and dynamic situations, for example, in a seismic event.

5. **Main axis drives**. The telescope drives track the telescope at control frequencies limited by the resonances of the natural vibration modes of the telescope structure. The inertial mass of the structure is relied upon to attenuate disturbances at frequencies above the maximum control frequency. Fast tip-tilt of the secondary mirrors provides the final level of jitter correction. The telescope main axis drives are required to apply smooth torque to the structure during tracking. The controllers will be designed to operate at control frequencies as high as possible while still remaining stable. The drives and controllers will be analyzed during the next development phase.

6. **Instrument Rotator**. The Instrument Rotator supports the weight of the Gregorian and folded port instruments and rotates to compensate for field rotation due to alt-azimuth tracking and slewing. Smooth operation and moderately high precision are required. The current concept uses rollers to support the load and constrain the motion but a regular bearing is an option being studied. Trade-off studies will be conducted in the next development phase.

7. **Shipping**. Many of the components of the telescope exceed in size and weight standard loads that are normally shipped around the world. This greatly complicates the logistics and cost of bringing the telescope to the site. Many of the telescope and auxiliary components will undergo fabrication, machining and assembly at different locations further complicating matters. A staging and shipping plan will be developed with fabricators and shipping companies during the next phase to assess the difficulty and cost entailed. Access to a nearby port with break-bulk service and large crane capacity will be a factor in selecting a fabricator, for example. Transportation in Chile is also an issue.

8. **Assembly on site.** Staging, handling and assembling the large telescope pieces on site will be challenging. The baseline site is laid out with large staging areas adjacent to the enclosure. Crane access through the enclosure shutter is possible but most of the assembly will be done with the overhead crane. Special fixturing will be required to move pieces into position and hold them in place during assembly. All of this will be planned out well in advance of the construction phase. The alternate sites may have much smaller staging areas which will affect the final plan.

9. **Earthquake safety**. Las Campanas Observatory is in a seismically active area. The GMT will be designed to earthquake standards specified in the Design Requirements Document. The telescope structure will be most vulnerable during assembly before all of the connections

and bracing are in place. During the year of assembly moderate earthquakes of magnitude 4 are likely and major events (m > 6) are possible. The assembly procedures and fixturing will be designed to prevent catastrophic damage to the structure and injury to workers in the event of a major earthquake. This will be quantified prior to letting contracts for the telescope.

7.10 **References**

Chivens, D. 2005, GMT Preliminary Design- Hydrostatic Bearings, Document 1131, GMT.

Smith, D. 2000, Gemini South Wind Data Viewer. http://www.aura-nio.noao.edu/studies /wind_tests1/tests/index.html

Gunnels, S., Davison, W., Cuerden, B., Hertz, E. 2004 in SPIE Conf. Ser. 5495, Astronomical Structures and Mechanisms Technology, ed. J.Antebi, & D. Lemke (Bellingham: SPIE), 20

Gunnels, S. 2003, Recent GMT Structural Analysis and Design, Document 1096-gmt3.pdf, GMT

Gunnels, S. 2004, Recent GMT Structural Analysis and Design, Document 141-gmt6.pdf, GMT

Gunnels, S. 2004, Status of Pier Design and Analysis, Rev 28, Document 1346-gmt7.pdf, GMT

Gunnels, S. 2004, Recent GMT Structural Analysis and Design, Document 175-gmt8.pdf, GMT

Gunnels, S. 2004, Update of Pier Design and Analysis, Document 1093-gmt9.pdf, GMT

Gunnels, S. 2004, FEA of C-Ring Hydrostatic Pads and Runner Bearing, Document 1090-gmt12.pdf, GMT

Gunnels, S. 2004, GMT optics motions due to rotating in the gravity field, Document 1087-gmt17.pdf, GMT

Johns, M. 2005, Optical Sensitivity Equations for use in the Dynamical Response Analysis for the Giant Magellan Telescope, Document 1114, GMT

Kan, F. 2005, GMT Dynamic Wind Response Study Report, Simpson, Gumperz, & Heger, Document 1356, GMT.

Smith, D and Avitabile, A. 2000, Gemini South 8m Optical Telescope, Final Report, MACL Report # 05-08570-001, University of Massachusetts at Lowell, Lowell, MA